NASA TECHNICAL NOTE

NASA TN D-8134 *c.l*

STUDY OF THE LOWER STRATOSPHERIC THERMAL STRUCTURE AND TOTAL OZONE FROM NIMBUS-4 IRIS

C. Prabhakara and E. B. Rodgers

Goddard Space Flight Center
Greenbelt, Md. 20771

1. Report No. NASA TN D-8134	2. Government Accession No.	3. Recipient's Catalog No.
4. Title and Subtitle Study of the Lower Stratospheric Thermal Structure and Total Ozone from Nimbus-4 IRIS		5. Report Date January 1976
		6. Performing Organization Code 910
7. Author(s) C. Prabhakara and E. B. Rodgers		8. Performing Organization Report No. G-7620
9. Performing Organization Name and Address Goddard Space Flight Center Greenbelt, Maryland 20771		10. Work Unit No.
		11. Contract or Grant No.
12. Sponsoring Agency Name and Address National Aeronautics and Space Administration Washington, D. C. 20546		13. Type of Report and Period Covered Technical Note
		14. Sponsoring Agency Code 911-175-20-4001

15. Supplementary Notes

16. Abstract
The global distribution of temperature in the stratosphere from 100 to 10 mbar and the total ozone in the atmosphere are remotely sensed from the Nimbus-4 IRIS measurements for a period of about one year. The temperature and ozone data are presented in the form of monthly mean global maps. The standard deviations of temperature and ozone with respect to zonal averages are calculated. The mean and the variable state of the stratosphere are discussed with the help of these observations. The lower stratosphere in the tropical regions reveals a significant wave number one pattern in the circulation. The Arctic and Antarctic stratospheric winter circulation regimes display a different behavior apparently due to the ocean and orographic differences.

17. Key Words (Selected by Author(s)) Satellite global ozone measurements, Remote sensing of temperature, Circulation in the polar regions	18. Distribution Statement Unclassified—Unlimited Cat. 47		
19. Security Classif. (of this report) Unclassified	20. Security Classif. (of this page) Unclassified	21. No. of Pages 35	22. Price* $3.75

CONTENTS

STUDY OF THE LOWER STRATOSPHERIC THERMAL STRUCTURE
AND TOTAL OZONE FROM NIMBUS-4 IRIS

C. Prabhakara and E. B. Rodgers
Goddard Space Flight Center
Greenbelt, Maryland

SUMMARY

The Nimbus-4 infrared interferometer spectrometer (IRIS) obtained a high resolution, 2.8-cm^{-1}, infrared spectra from 80°N to 80°S during the period April 1970 to January 1971. These measurements were inverted to obtain temperature profiles and total amounts of ozone in a column of the atmosphere. The temperatures and total amounts of ozone obtained simultaneously from one instrument on board this earth-orbiting satellite have allowed the examination of the mean state of the stratosphere and its variability (on a global basis) for about one year. Global maps of monthly mean total ozone and temperature at the 100-, 50-, 30-, and 10-mbar levels were generated. Zonal means and the standard deviation for each of the above variables were computed.

The zonal mean temperatures display an annual cycle everywhere except at 10 mbar in the tropics where a semiannual cycle was observed. Striking asymmetries between north and south polar regions are apparent. The peak-to-peak amplitude of the annual temperature wave is about 30 K at 100 mbar and 40 K at 10 mbar over high latitudes in the north, while in the south polar region, the amplitude is 45 K at all levels. Maximum temperatures occur at all levels in both hemispheres near the summer solstice. However, at 100 mbar, the minimum temperatures occur near the winter solstice in the north polar region, but about one month after the winter solstice in the south polar region. At 10 mbar, the minimum occurs about one month before the winter solstice in the north polar region but is coincident with winter solstice in the south polar region.

The standard deviation of temperature, with respect to the zonal monthly mean, shows that throughout the year there is little fluctuation in the stratospheric temperatures in the tropics and subtropics. However, pronounced maxima are observed in polar regions at all levels. These maxima occur over the Arctic during the winter months while over the Antarctic, these maxima occur during the spring season.

Examination of the monthly mean maps indicates that these large standard deviations at the polar regions are associated with the stationary waves. The troughs and ridges of these waves are found to have a southwest to northeast tilt in the Northern Hemisphere, and a northwest to southeast tilt in the Southern Hemisphere, which is consistent with the poleward transport of heat and momentum.

The winter westerly polar vortex over the Antarctic is observed to be considerably stronger than that over the Arctic. However, no sudden warming events in the lower stratosphere (such as those observed over the Arctic) are seen during Antarctic winter. The lack of such warmings over the Antarctic appears to be due to the absence of the troposphere forcing.

Monthly mean total ozone maps reveal the planetary scale waves that are observed in the temperature maps of 100 mbar and 30 mbar. Apparently the large scale circulation is responsible for both the temperature and ozone patterns.

In the tropics, the ozone data suggest the presence of a wave number one pattern in the lower stratosphere with a maximum over the Atlantic region and a minimum over Southeast Asia. The geographic extent of the minimum ozone seems to grow in size in July, extending over the Tibetan plateau to the north. This particular development is apparently linked to the summer southwest monsoon and the Easterly jet stream that dominate the circulation over Southeast Asia.

The zonal mean total ozone in the middle and higher latitudes of the Northern Hemisphere displays an annual cycle with a maximum in the spring and minimum in the fall. In the tropics of the Northern Hemisphere, the phase of this annual cycle appears to be opposite. The midlatitudes of the Southern Hemisphere show a maximum in spring and minimum in fall, but the south polar region reveals quite a different seasonal change. South of 60°S, a secondary minimum occurs in May with a principal minimum occurring in September, followed by a strong maximum in November and December. It is interesting to note that this increase in ozone results from the transport processes produced by the intense wave activity which is revealed by the standard deviation in the temperature data.

INTRODUCTION

The Nimbus-4 infrared interferometer spectrometer (IRIS) has obtained high resolution, 2.8-cm^{-1}, infrared spectra from 80°N to 80°S during the period April 1970 to January 1971. This instrument has a field-of-view of approximately 95 km at nadir. A detailed discussion of the measurements and calibration techniques used to obtain these data is presented by Hanel et al. (1972). The intensity measurements in the 15-μm region have been inverted to obtain temperature profiles over the globe. When the 9.6-μm intensities measured by IRIS are used in conjunction with the temperature profile, it is possible to estimate the total amount of ozone in a column of the atmosphere. These measurements of temperature and total ozone, obtained simultaneously from one instrument on board this earth-orbiting satellite, are used to examine the mean state of the stratosphere and its variability (on a global basis) for approximately one year.

REMOTE SENSING TECHNIQUE

The temperature sounding from the satellite 15-μm CO_2 band radiance measurements is done in the present study following the minimum information method developed by Conrath and

Revah (1972).* The initial guess profile needed for this method is based directly on the measured radiances. This is done by taking advantage of the fact that the weighting functions for different spectral intervals tend to peak at different pressures in the atmosphere. For a first approximation, the brightness temperature in a given spectral interval of the band may be associated with the temperature at a pressure level corresponding to the peak in the weighting function. The most opaque part of the 15-μm IRIS spectrum is at 667.5 cm^{-1}. The weighting function for this spectral interval has a broad maximum around 17 mbar. Thus, the initial temperature profile can be readily specified up to that level. However, in the 667.5-cm^{-1} region, a significant amount of emission from the atmosphere up to the level of 10 mbar is present. In the present study, an attempt is made to derive temperatures up to 10 mbar. This requires some way of prescribing the initial temperature structure to considerably lower pressures. Based upon the climatological character of the temperature profile in the stratosphere, it is assumed that the temperature increases linearly with height up to 3 mbar. Because the initial temperatures are available at heights below 17 mbar directly from radiances, temperatures at 3 mbar can be estimated by extrapolation, with the help of the above assumption. The brightness temperature in the 950-cm^{-1} window region of the spectrum is assumed to give the surface temperature with no correction for cloud contamination in the data.

The temperature profile retrieved from the 15-μm radiances, with the initial guess as described above, is found to be free of cloud effects above approximately 200 mbar. In the troposphere below this level, the cloud contamination can make the temperature measurement unreliable. Further, in the remote temperature sensing, the tropopause structure is grossly smoothed because the height resolution of the retrieved temperature profile is several kilometers (Conrath, 1972). Despite these limitations, the stratospheric temperatures derived here for a period of about one year show a good systematic behavior in time and space. This self-consistency of data has allowed this study to be made.

The remote sensing of total ozone from the 9.6-μm IRIS intensities has been demonstrated by Prabhakara et al. (1970). The temperature sounding from the 15-μm data is needed for the remote sensing of ozone. The emissivity characteristics of the surface of the earth (such as the silicon dioxide emissivity band over a desert surface) or of clouds can affect the 9.6-μm band intensities measured from space. These spectral impurities are systematically eliminated following the procedure of Prabhakara et al. (1972). Thereafter, the total ozone is estimated from essentially one piece of information contained in the entire 9.6-μm band, as explained in the appendix.

The total ozone, measured from April 1970 to January 1971, is compared at a few Dobson ozone measuring stations over the globe. In figures 1 and 2, a comparison is shown for Arosa and MacQuarie Island. The IRIS-derived total ozone varies with time, as do the Dobson measurements, at both stations. However, a close examination reveals that the IRIS data underestimate ozone in the spring months and overestimate ozone in the fall months, thereby reducing the annual amplitude in the ozone cycle. This, apparently, is the limitation of the

---

*Conrath, B. J. and I. Revah, "A Review of Non-statistical Techniques for the Estimation of Vertical Atmospheric Structure from Remote Infrared Measurements," in *Proceedings of a Workshop on the Mathematics of Profile Inversion* (L. Colin, ed.), NASA TM X-62150, 1972.
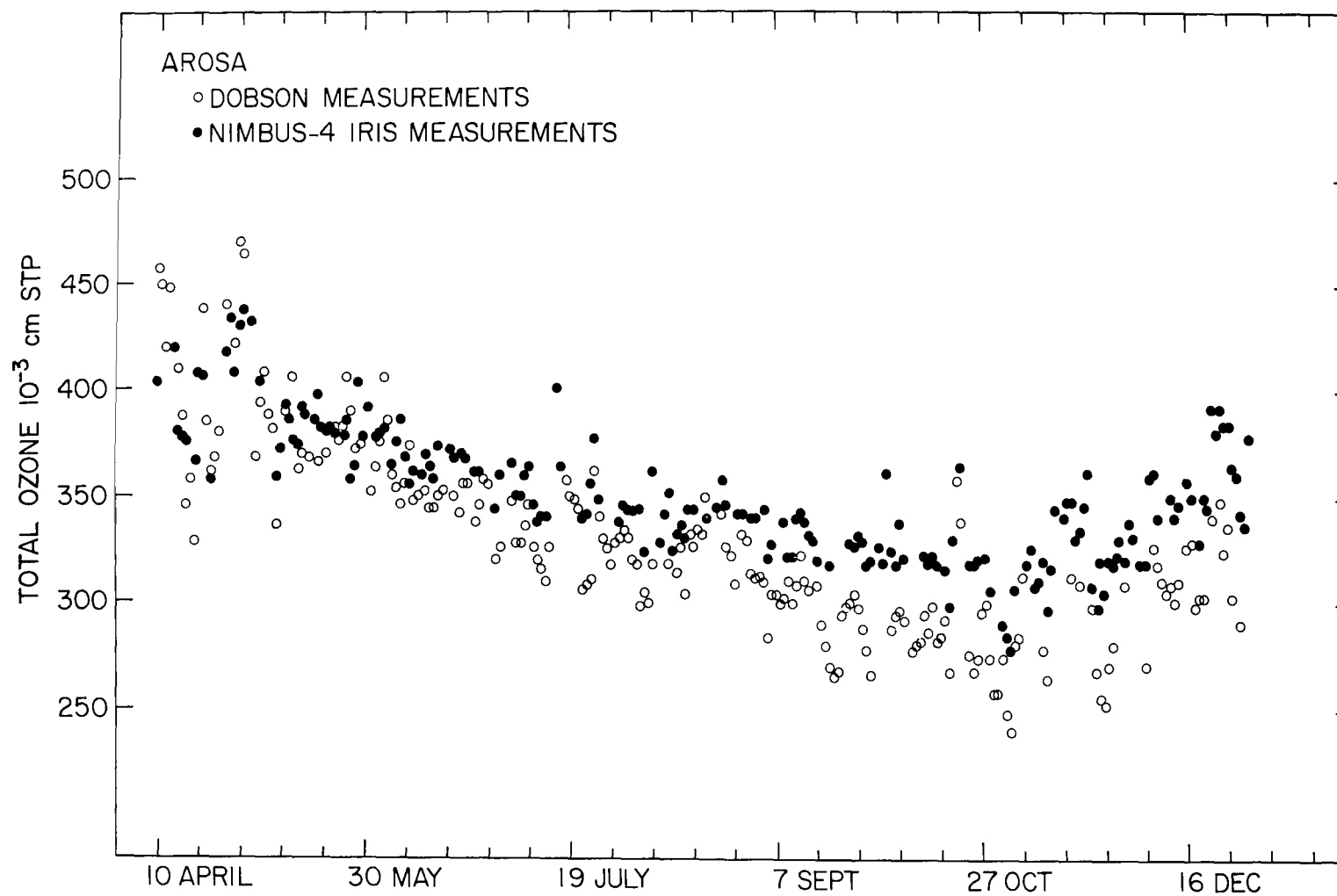
Figure 1. Daily observation of total ozone (10^{-3}-cm STP) obtained from Dobson measurements (o) and Nimbus-4 IRIS measurements (●) for Arosa, Switzerland, from April 10 to December 31, 1970.
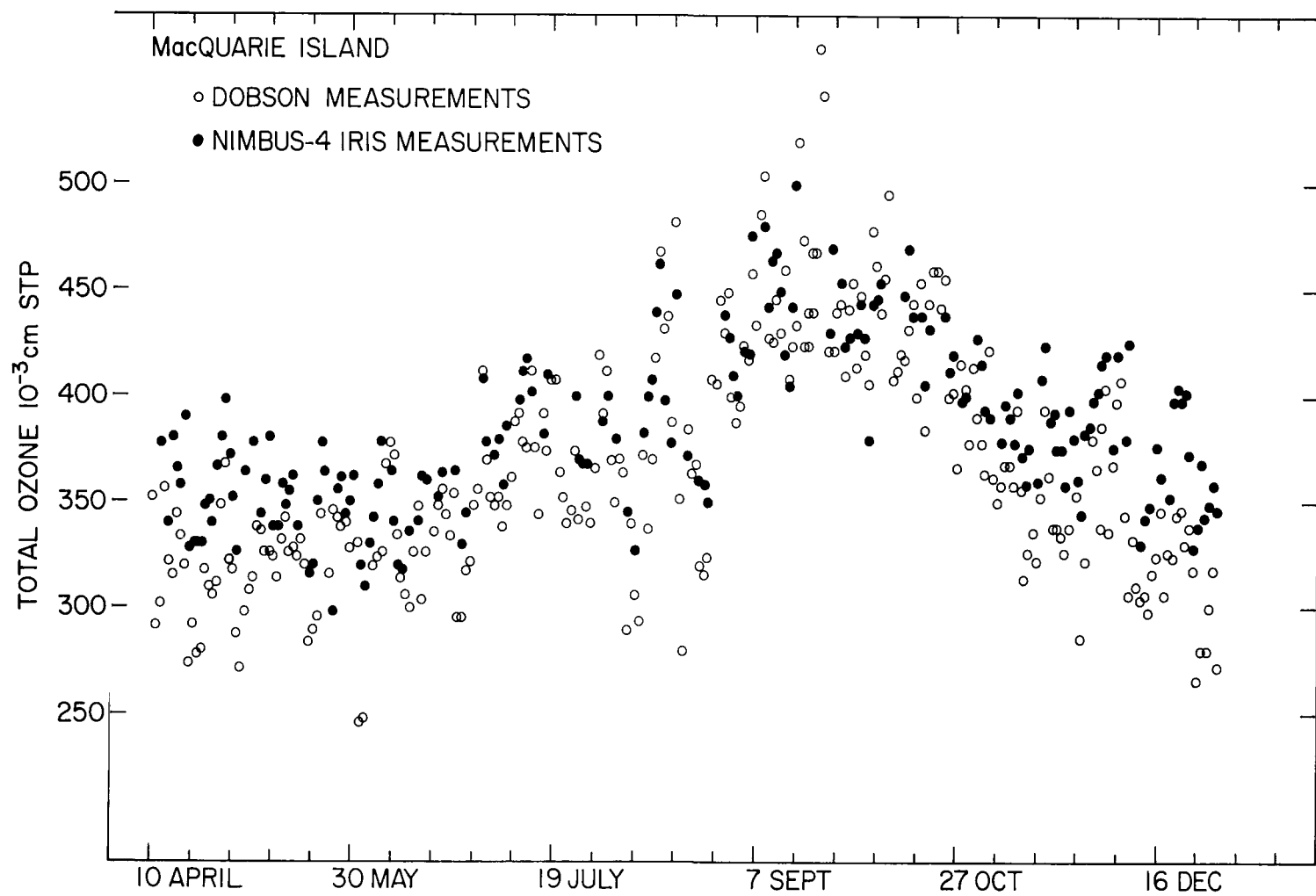
Figure 2. Daily observation of total ozone (10^{-3}-cm STP) obtained from Dobson measurements (o) and Nimbus-4 IRIS measurements (●) for MacQuarie Island from April 10 to December 31, 1970.

one parameter remote ozone sensing method in the infrared. Despite this systematic error in the data, one can study temporal and spatial variations in the global ozone field in association with changes in circulation patterns.

THERMAL STRUCTURE OF THE LOWER STRATOSPHERE

The temperature measurements were made by IRIS in the stratosphere at four levels (100, 50, 30, and 10 mbar) for the period April 1970 to January 1971. These measurements were analyzed to provide:

- Monthly mean temperature maps

- Monthly zonal mean temperatures, and

- Standard deviation of temperature as a function of latitude for each month.

Examination of the temperature data in this manner readily permits one to appreciate the thermal variations of the stratosphere at different spatial and temporal scales.

Several earlier studies, (Labitske and Van Loon, 1972; Crutcher, 1970) based on conventional temperature measurements, have revealed the broad features of the stratospheric thermal field. Also, some further understanding of the stratospheric character was obtained from satellite measurements (see, for example, Adler, 1975; Quiroz, 1975; and Barnett, 1974). In this study an attempt was made to show the mean thermal field of the global stratosphere, month by month, and its variability from the zonal monthly mean by using satellite sensing techniques. This information is helpful in examining the evolution of the circulation patterns in conjunction with the thermal field.

Monthly Mean Temperature Maps

Global maps of monthly mean temperature at the four different levels are presented in figures 3 through 11. The January 1971 map is not included, because only 10 days of data were available for this month. Generally, at the 10-mbar level (the highest level in these observations), the thermal field shows strong solar control with warm temperatures during summer solstices and cold temperatures during winter solstices. In the lower layers of the atmosphere, the solar control is observed to be less pronounced, and the large scale circulation of the atmosphere begins to influence the thermal field. This is evidenced by the large standing wave systems that are present in the Northern and Southern Hemispheres. Primarily, these monthly mean temperature maps in the lower stratosphere reveal wave number one. Wave number one dominates the Northern Hemisphere circulation during the fall months over a wide latitudinal band (40°N to pole) with a maximum temperature over Manchuria and a minimum temperature over Europe. On constant pressure surfaces, the troughs and ridges of the temperature patterns have a NE-to-SW tilt. They slope westward with height with decreasing amplitude in the wave. With the progressive cooling of the polar regions during winter, this standing wave system intensifies considerably with little change in its geographic location.

6
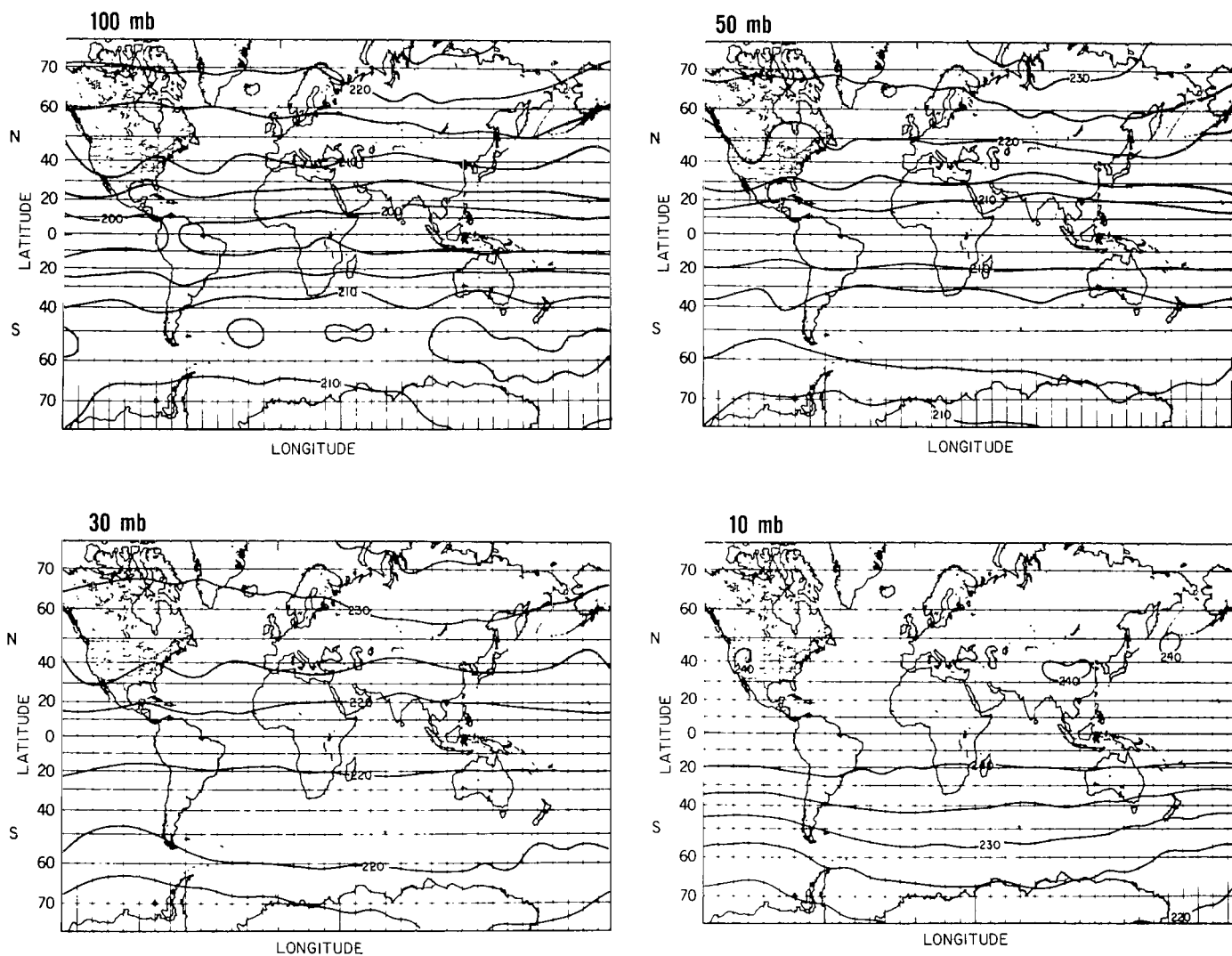
100 mb

50 mb

30 mb

10 mb

Figure 3. Global distribution of stratospheric temperature (K) derived from Nimbus-4 IRIS measurements at 100, 50, 30, and 10 mbar for April 1970.
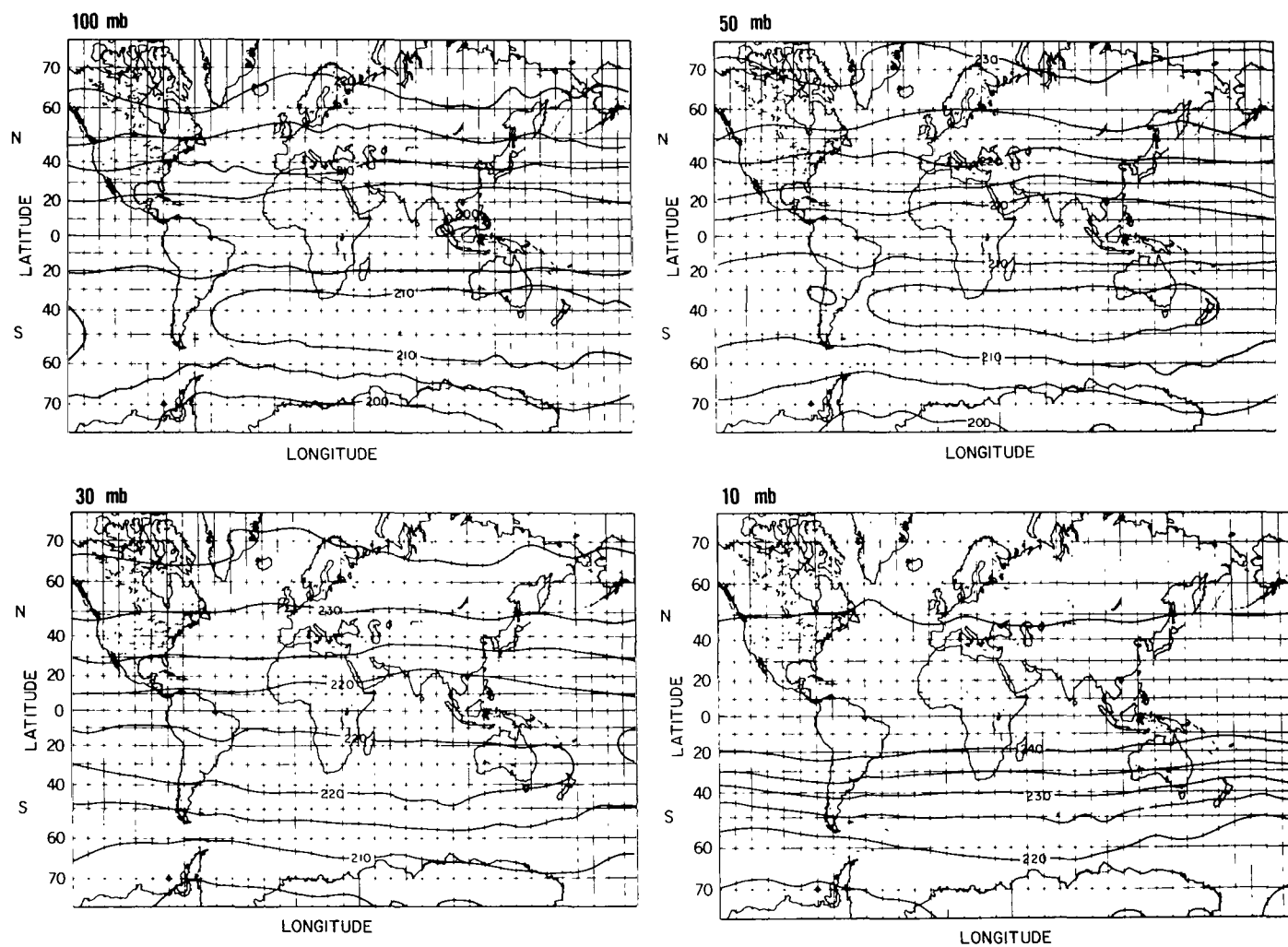
Figure 4. Global distribution of stratospheric temperature (K) derived from Nimbus-4 IRIS measurements at 100, 50, 30, and 10 mbar for May 1970.
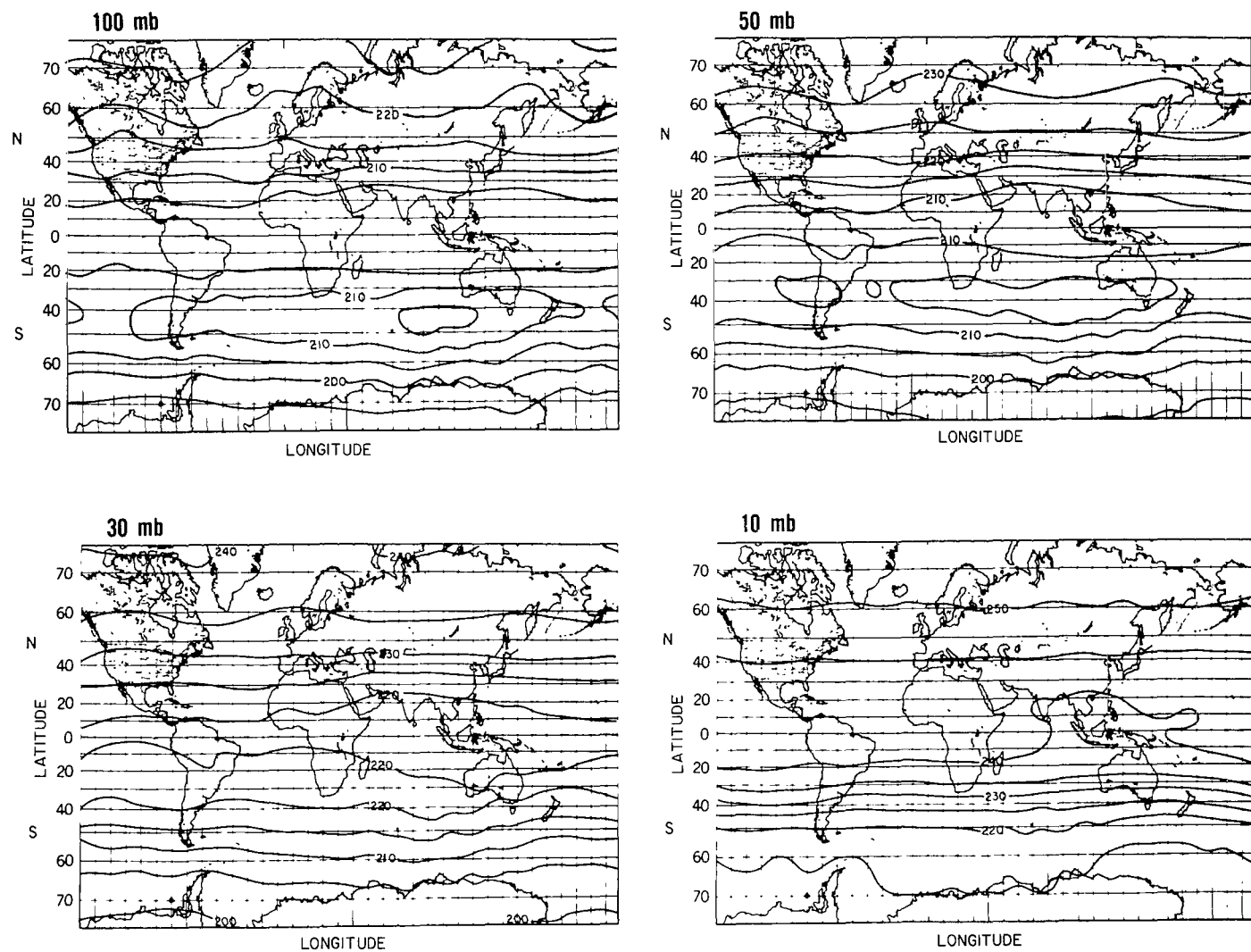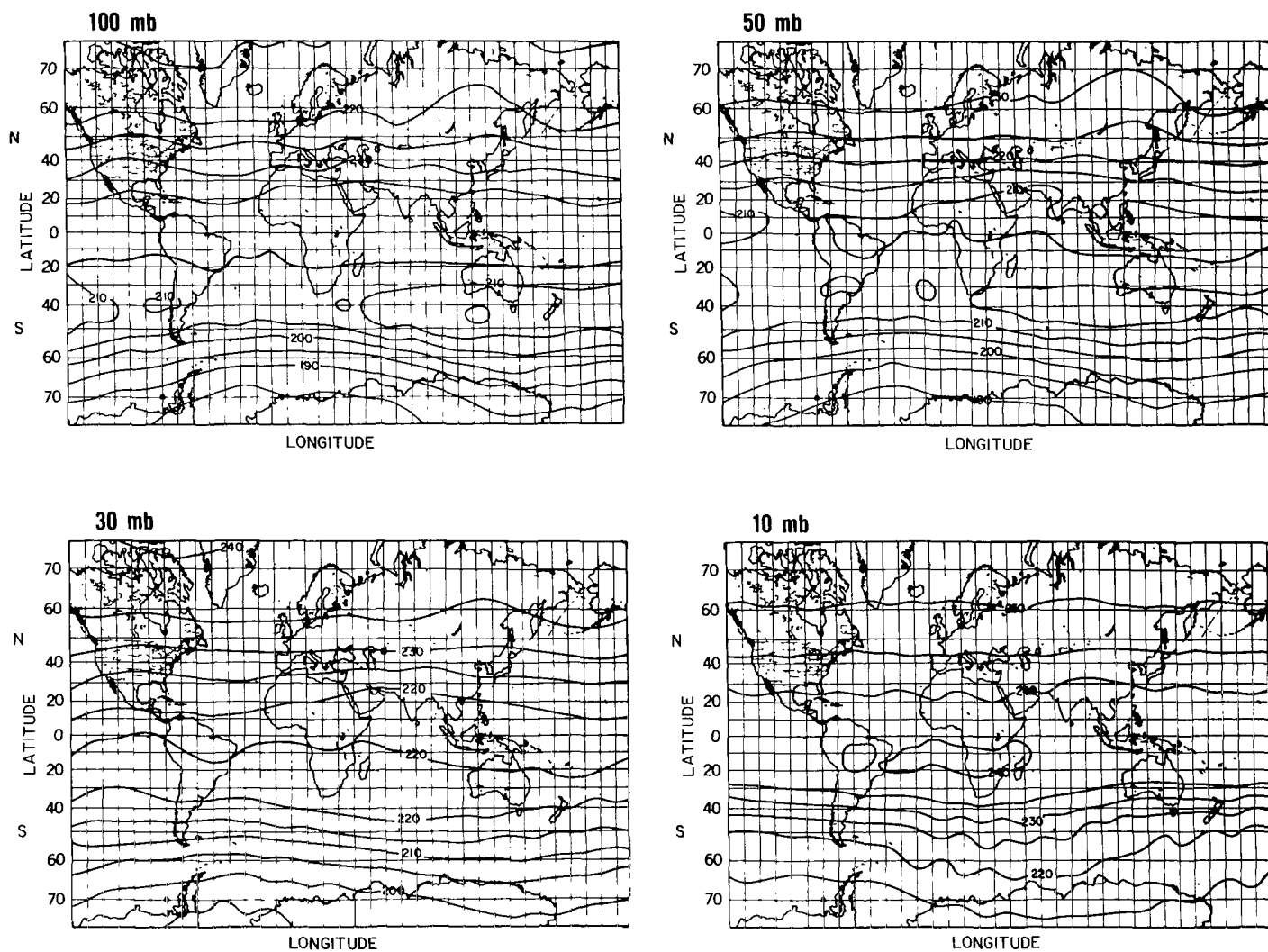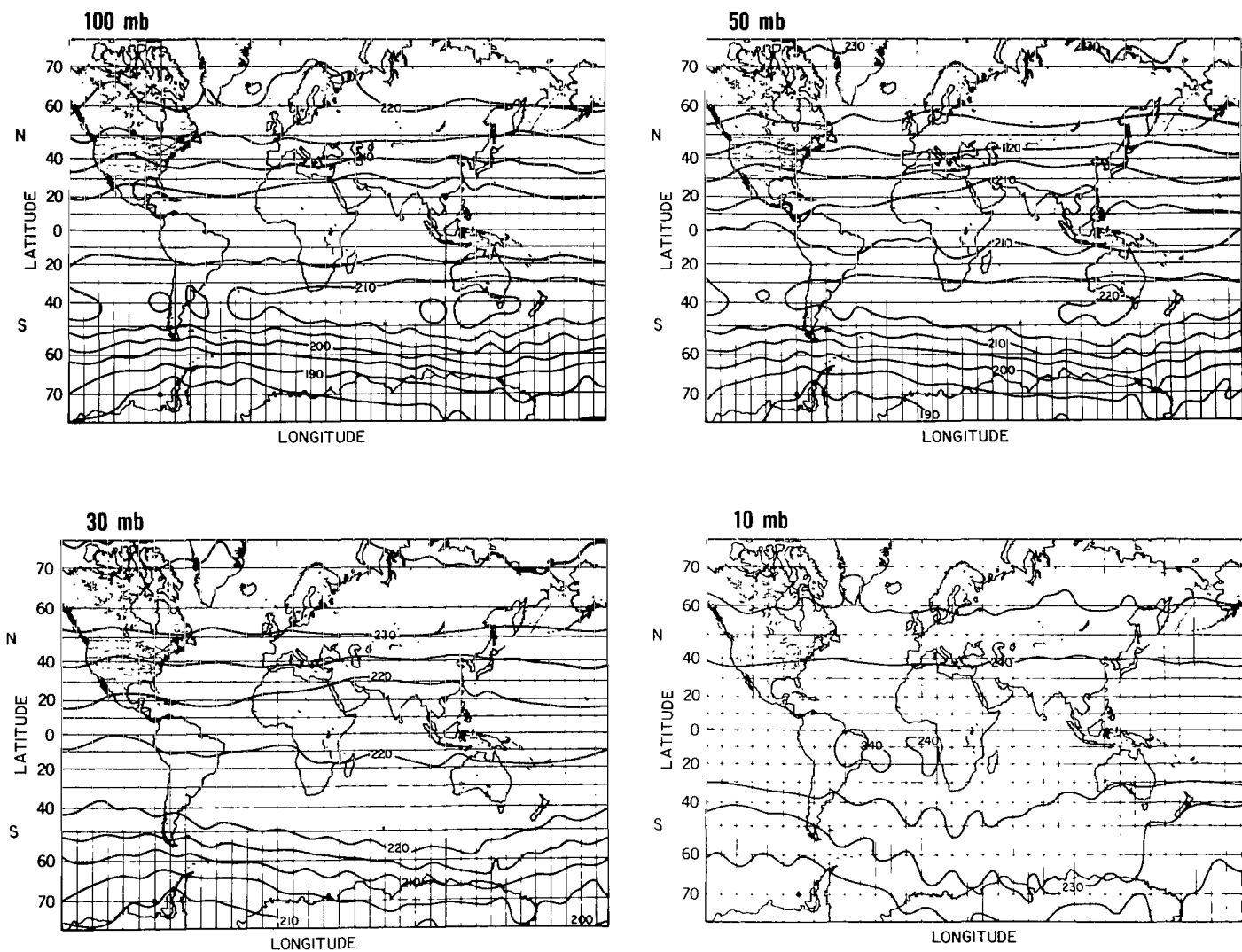
100 mb

50 mb

30 mb

10 mb

Figure 5. Global distribution of stratospheric temperature (K) derived from Nimbus-4 IRIS measurements at 100, 50, 30, and 10 mbar for June 1970.

6

100 mb

50 mb

30 mb

10 mb

Figure 6. Global distribution of stratospheric temperature (K) derived from Nimbus-4 IRIS measurements at 100, 50, 30, and 10 mbar for July 1970.

100 mb

50 mb

30 mb

10 mb

Figure 7. Global distribution of stratospheric temperature (K) derived from Nimbus-4 IRIS measurements at 100, 50, 30, and 10 mbar for August 1970.
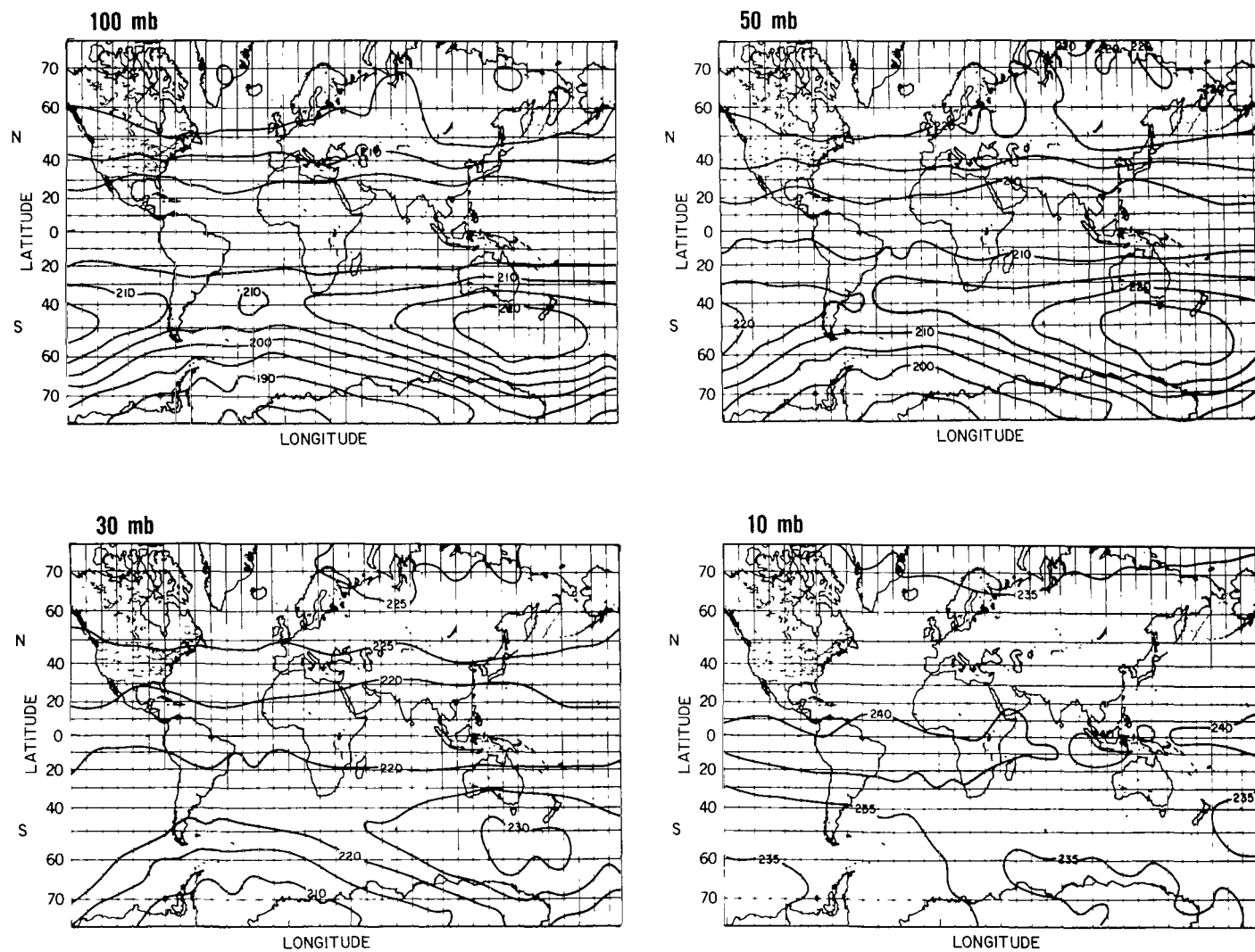
Figure 8. Global distribution of stratospheric temperature (K) derived from Nimbus-4 IRIS measurements at 100, 50, 30, and 10 mbar for September 1970.
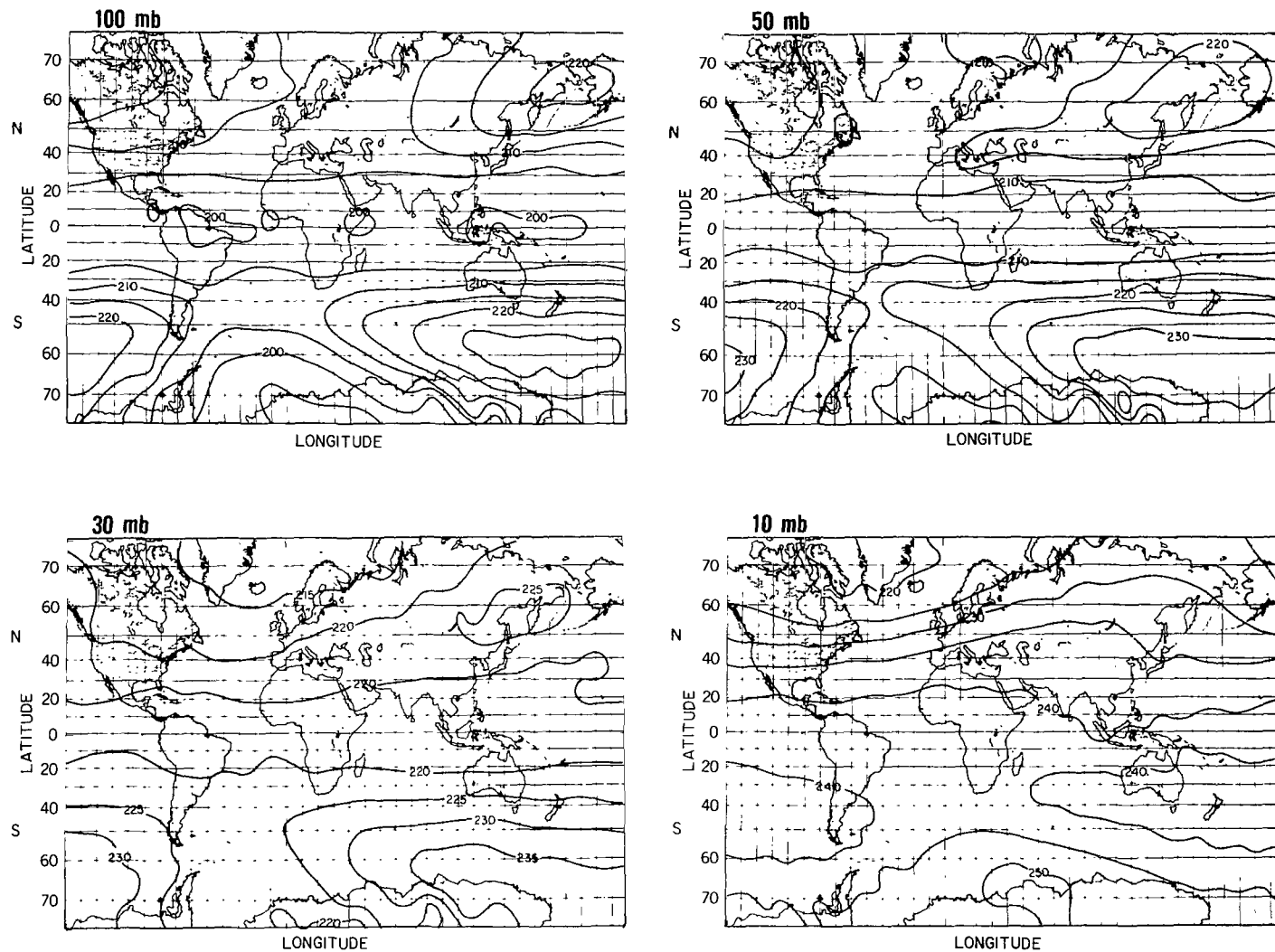
Figure 9. Global distribution of stratospheric temperature (K) derived from Nimbus-4 IRIS measurements at 100, 50, 30, and 10 mbar for October 1970.
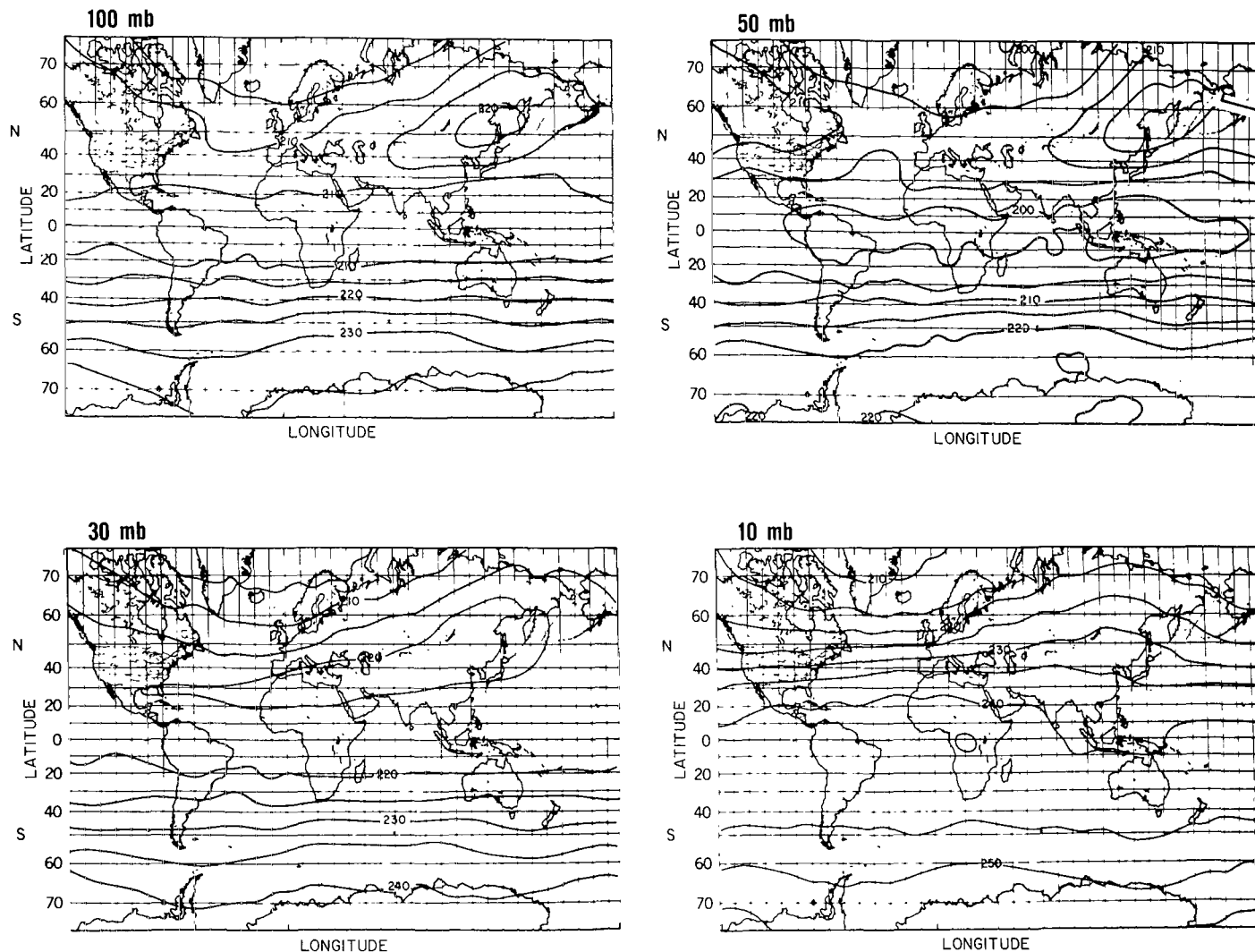
100 mb

50 mb

30 mb

10 mb

Figure 10.   Global distribution of stratospheric temperature (K) derived from Nimbus-4 IRIS measurements at 100, 50, 30, and 10 mbar for November 1970.
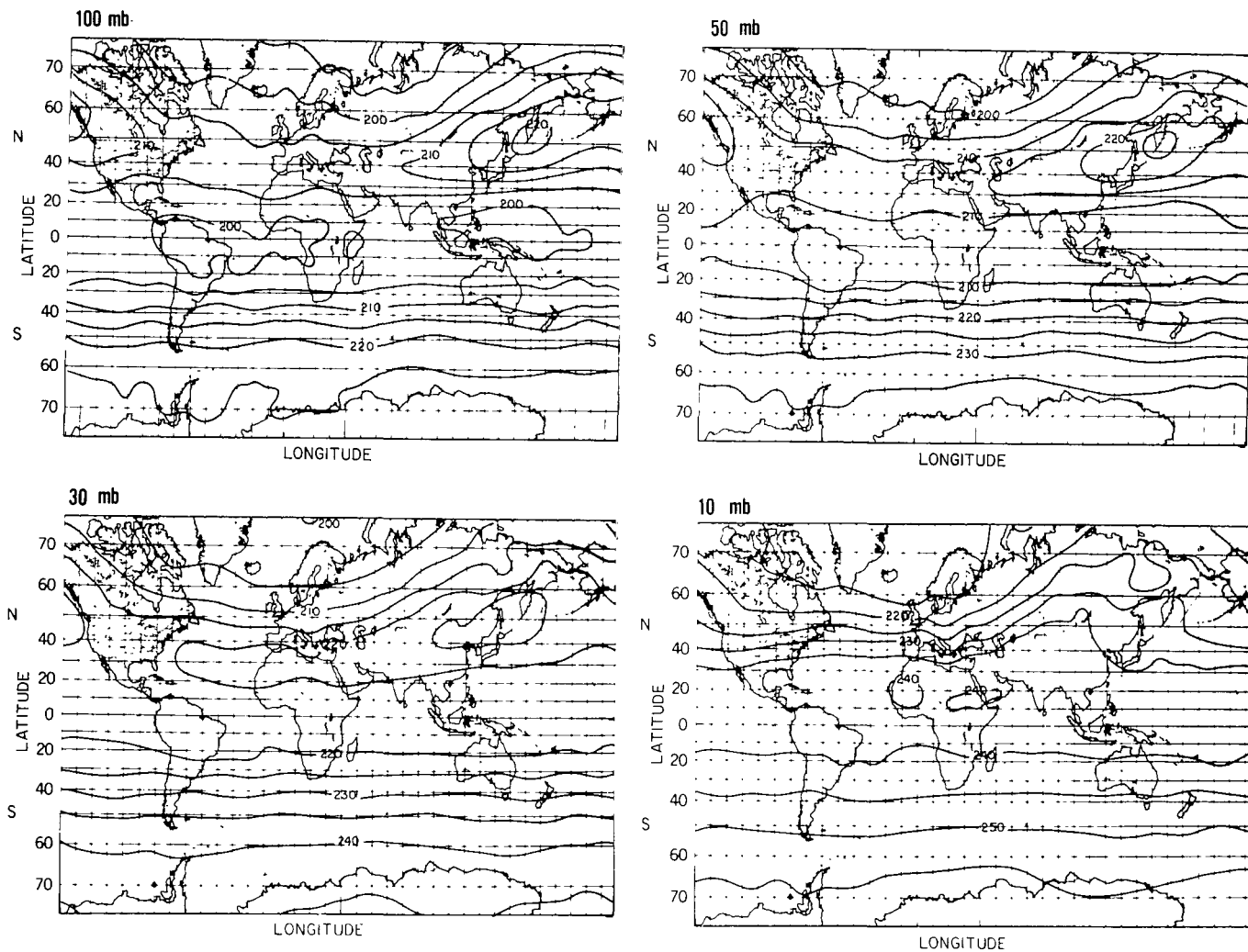
Figure 11. Global distribution of stratospheric temperature (K) derived from Nimbus-4 IRIS measurements at 100, 50, 30, and 10 mbar for December 1970.

In the Southern Hemisphere, the standing wave number one in the temperature field is confined to middle latitudes in winter months. The temperature maximum is seen primarily south of Australia in the lower stratosphere with lower temperatures over South America. The westward slope with height of the trough and ridge system is not noticeable in winter. However, later in the spring, wave number one acquires maximum strength, migrates closer to the South Pole, and a westward tilt with height is observed. This delayed behavior of the Southern Hemisphere stratosphere is in striking contrast to that of the Northern Hemisphere.

Monthly Zonal Mean Temperatures

In order to appreciate the global and seasonal temperature variability, the zonal averages for each month at the four levels—100, 50, 30, and 10 mbar—are plotted in figure 12 as a function of latitude and month. An annual cycle in the temperature field at all levels and latitudes is noted. However, in the tropics at the 10- and 30-mbar levels, a semiannual cycle with an amplitude of approximately 2°C may be observed. The amplitude of the annual cycle is approximately 30°C at all levels over the northern high latitudes, while it is considerably larger (approximately 45°C) over the southern polar regions. This large amplitude is produced by the more intense heating in the Southern Hemisphere summer (since the sun is closer to the earth during the Southern Hemisphere solstice) and the more intense cooling in the winter over the southern polar region (due to the enhanced radiative cooling from the high and cold Antarctic plateau).

Temperature maxima at all levels in both hemispheres occur in the summer months. However, the temperature minima are observed to occur earlier at the 10-mbar level and somewhat later at 100 mbar. This effect is particularly conspicuous at polar latitudes. In the north, at 10 mbar, the minimum is seen during November, and, about a month later, it appears at 100 mbar. This suggests that the minimum (at all levels) is produced either in early or middle winter. In the Southern Hemisphere, the minimum at 10 mbar occurs during the June and July period, while at 100 mbar, it is observed in August. In comparison with the Northern Hemisphere, the Southern Hemisphere has a delayed sequence of events. The stratospheric warmings, which are present in the Northern Hemisphere during winter, but absent in the Southern Hemisphere during winter, apparently are responsible for this.

Standard Deviation of Temperature

The standard deviation of temperature (with respect to the zonal monthly mean) is calculated from IRIS data for the four stratospheric levels and is plotted as a function of latitude and month in figure 13. The variability of the temperature, indicated by standard deviation, gives a measure of the energy contained in the standing waves. The tropical regions, in general, indicate weak activity of the waves in the stratosphere throughout the year. In the middle and high latitudes, the pronounced activity of the waves is manifested with the exception of the summer months. In the northern polar region, the wave activity reaches a maximum of about 11°C standard deviation during December and January. The standard deviation remains nearly constant with height up to the 10-mbar level. In the southern
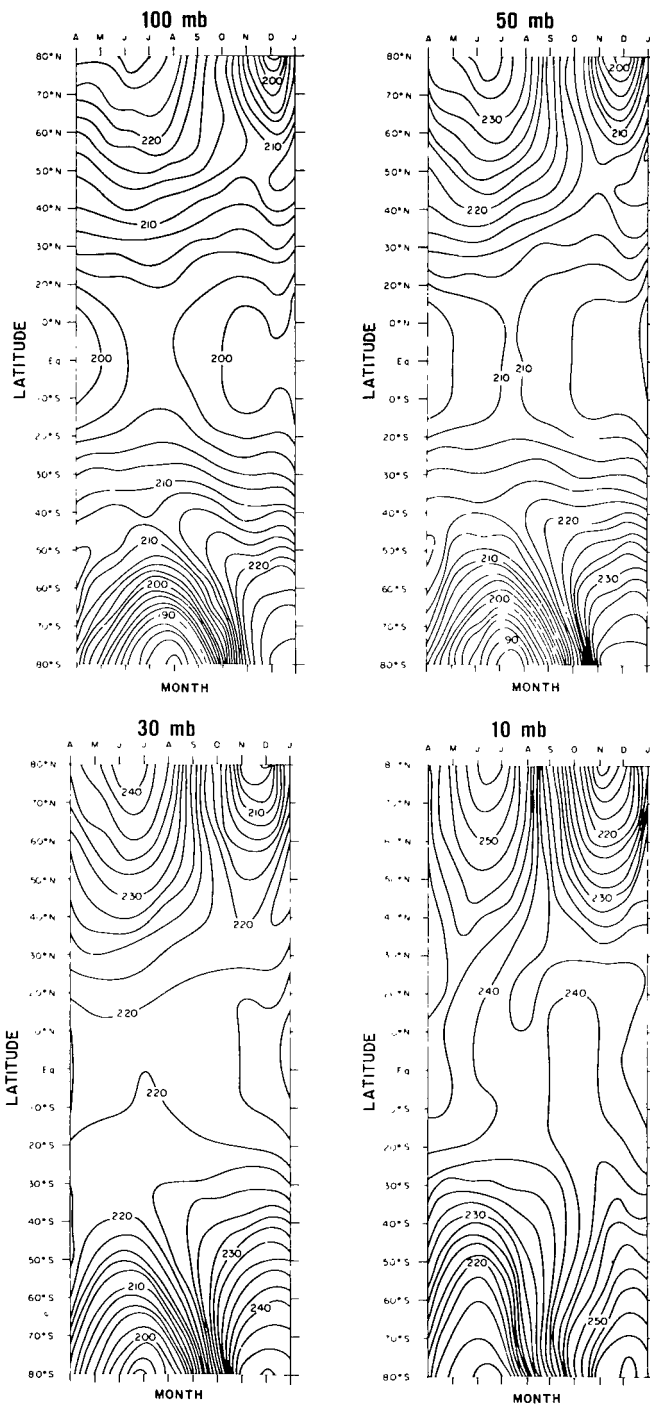
Figure 12. Zonal average stratospheric temperature (K) derived from Nimbus-4 IRIS measurements for April 1970 through January 1971 at 100, 50, 30, and 10 mbar.
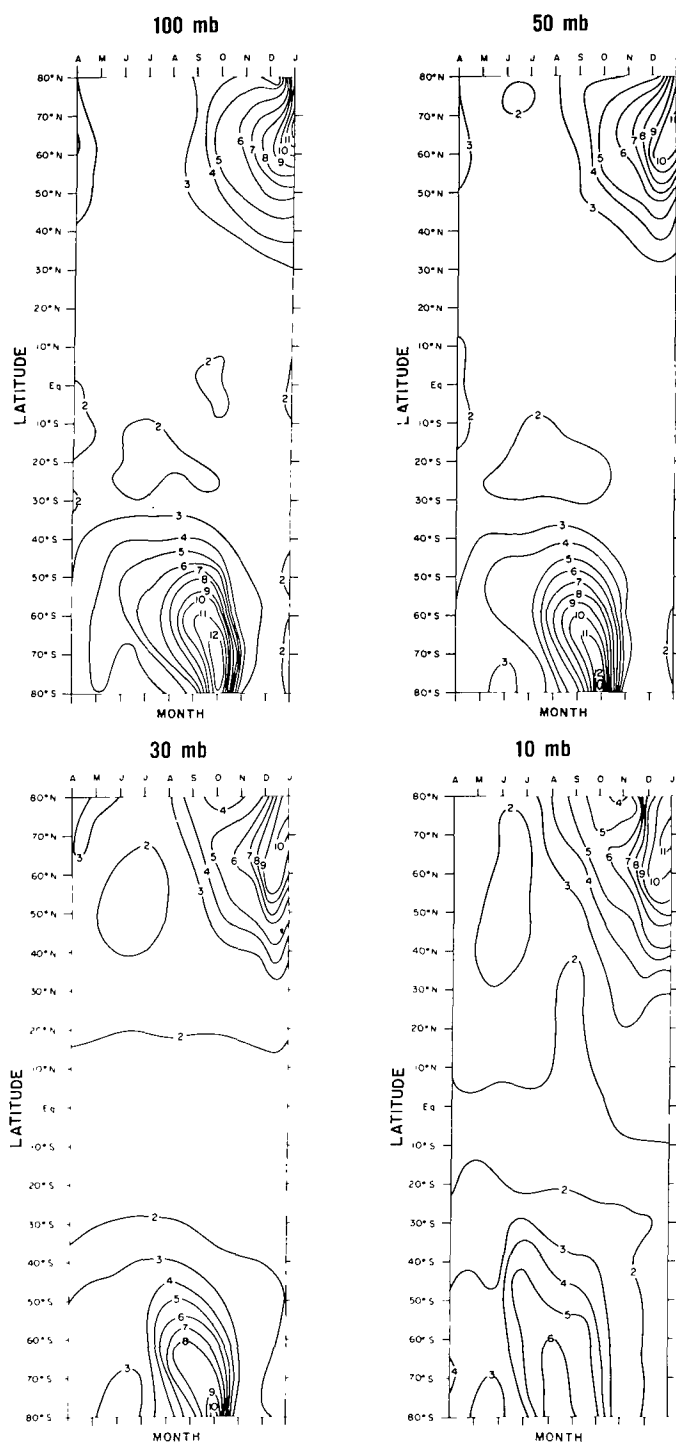
Figure 13. Standard deviation of stratospheric temperature (K) with respect to the zonal monthly mean derived from Nimbus-4 IRIS measurements for April 1970 through January 1971 at 100, 50, 30, and 10 mbar.

18

hemispheric polar region between the 100- and 30-mbar levels, the largest values of standard deviation are observed in October. Further, the magnitude of the standard deviation decreases from about 10°C at 100 mbar to about 9°C at 30 mbar. The 10-mbar level has a maximum standard deviation of only 6°C during the period of late August and early September.

TOTAL OZONE MEASUREMENTS FROM IRIS

The total ozone measured by IRIS is analyzed, analogous to the temperature, to give:

- Monthly mean maps

- Zonal mean, and

- Standard deviation as a function of latitude and month.

Such analyses complement the information revealed by the temperature data. The importance of ozone in the understanding of the stratospheric circulation on a global scale was demonstrated by several earlier studies (see, for example, Bojkov, 1968; London, 1963; Dutsch, 1969). However, in the earlier studies, ozone data available from conventional ground-based measurements were quite sparce and limited to continental areas. The satellite measurements that are presented here eliminate several inadequacies of ground-based measurements and permit one to obtain a good objective analysis.

Monthly Mean Maps

From the ozone maps shown in figures 14 through 22, it is observed that at middle latitudes, ozone is at maximum during the spring months and at minimum during the fall in both hemispheres. In association with the maxima, the latitudinal gradient increases and, conversely, with minima, it decreases. In the tropics, the total ozone changes approximately 10 Dobson units (D.U.) during the course of the year with a maximum in the July through August period and a minimum in April.

A significant ozone maximum begins to develop over Manchuria during October and intensifies through December with a corresponding minimum over the North Atlantic region. This standing wave number one pattern closely reflects the temperature patterns shown in the previous section. Again, in the Southern Hemisphere, ozone maximum south of Australia and the minimum in the South Atlantic in October bear a close resemblance to the corresponding temperature data. Apparently, large scale circulation is associated with the standing wave number one, generating both the temperature and ozone patterns.

In the tropics, the ozone data suggest the presence of standing wave number one with a maximum over the Atlantic region and a minimum over Southeast Asia. The geographic extent of the ozone minimum appears to increase in size somewhat, in the July through August period, extending over the Tibetan plateau to the north. This particular development is apparently linked to the summer southwest monsoon and to the easterly jet stream that dominates the circulation over Southeast Asia during that season.
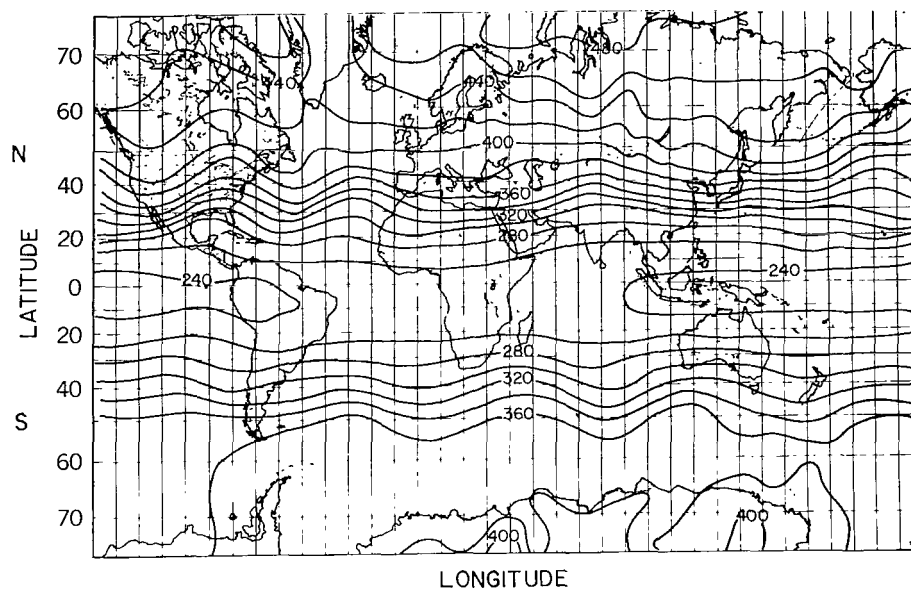
Figure 14. Global distribution of total ozone (Dobson units) derived from Nimbus-4 IRIS measurements for April 1970.
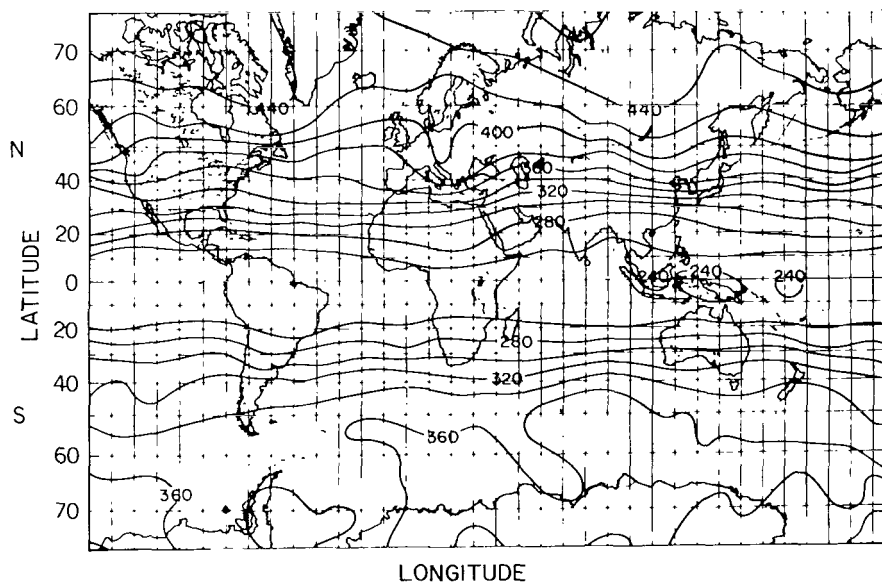

Figure 15. Global distribution of total ozone (Dobson units) derived from Nimbus-4 IRIS measurements for May 1970.
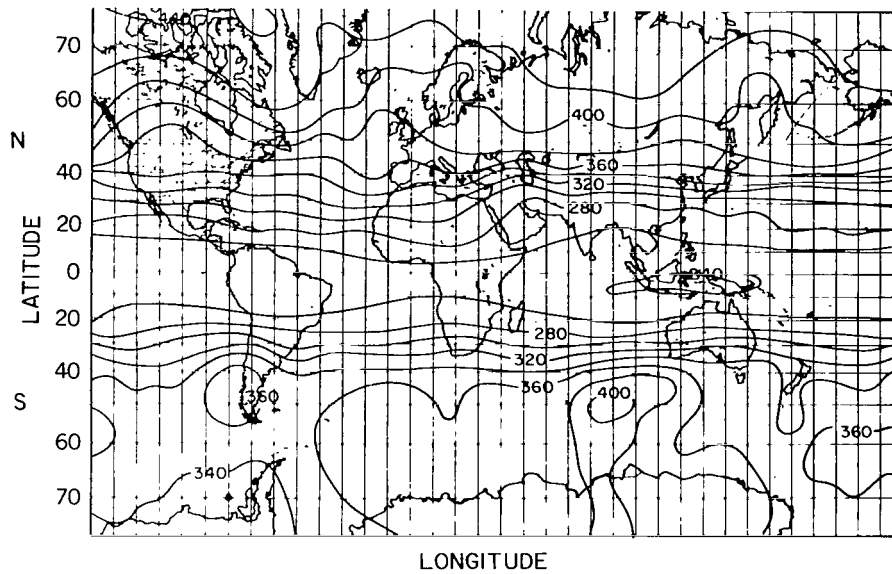
Figure 16. Global distribution of total ozone (Dobson units) derived from Nimbus-4 IRIS measurements for June 1970.
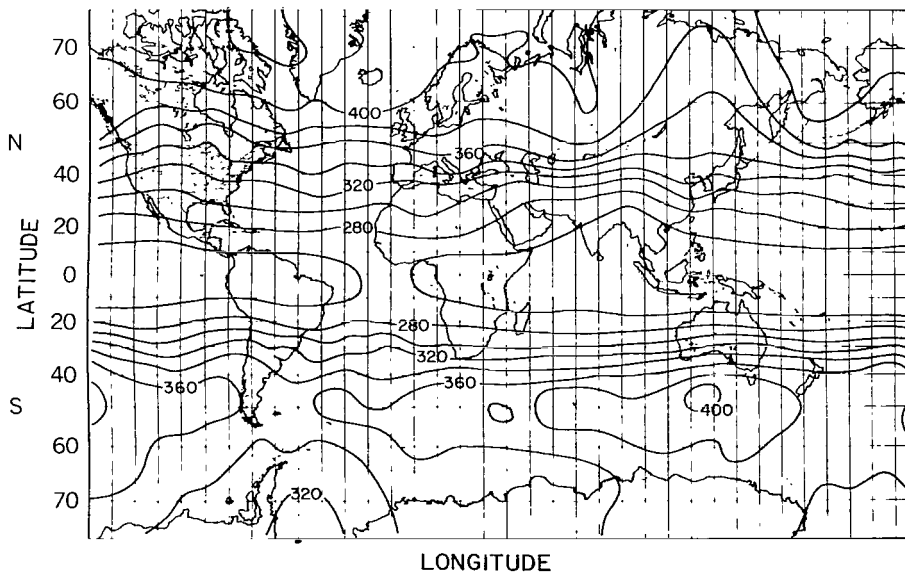

Figure 17. Global distribution of total ozone (Dobson units) derived from Nimbus-4 IRIS measurements for July 1970.
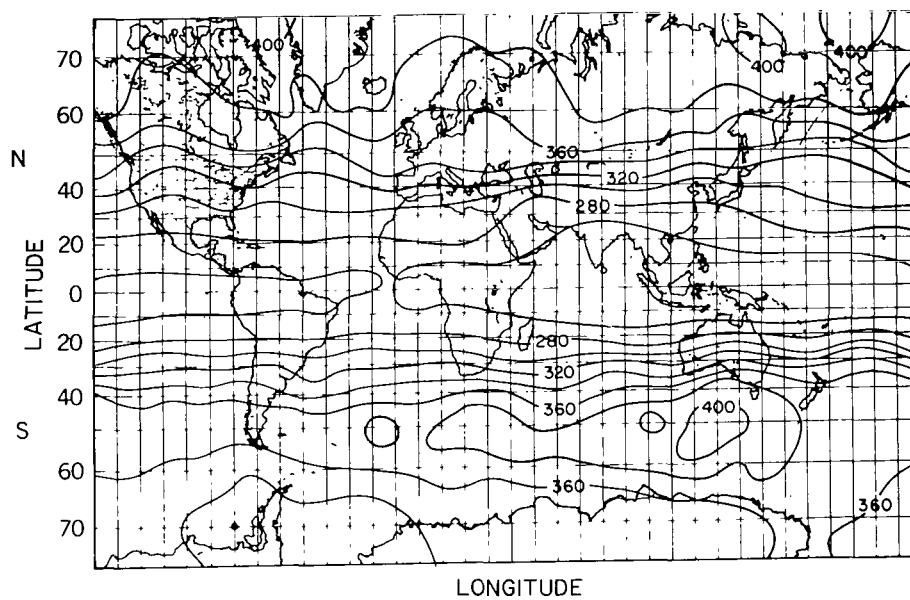
Figure 18. Global distribution of total ozone (Dobson units) derived from Nimbus-4
IRIS measurements for August 1970.

Figure 19. Global distribution of total ozone (Dobson units) derived from Nimbus-4
IRIS measurements for September 1970.

22

Figure 20. Global distribution of total ozone (Dobson units) derived from Nimbus-4 IRIS measurements for October 1970.
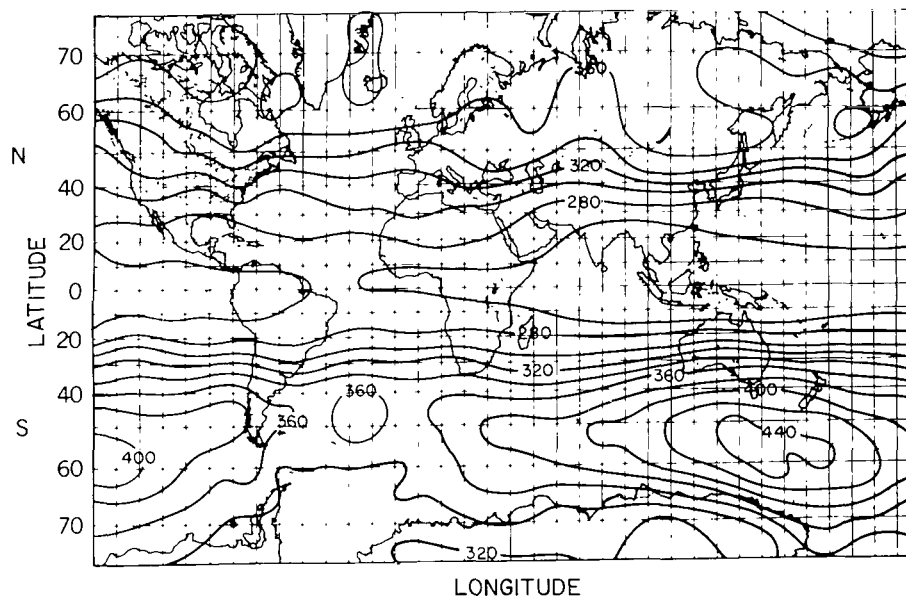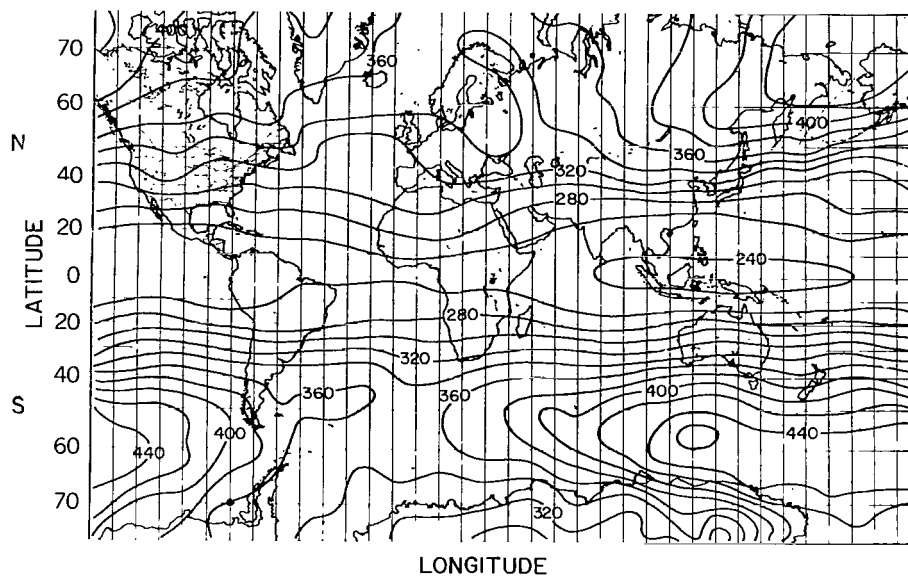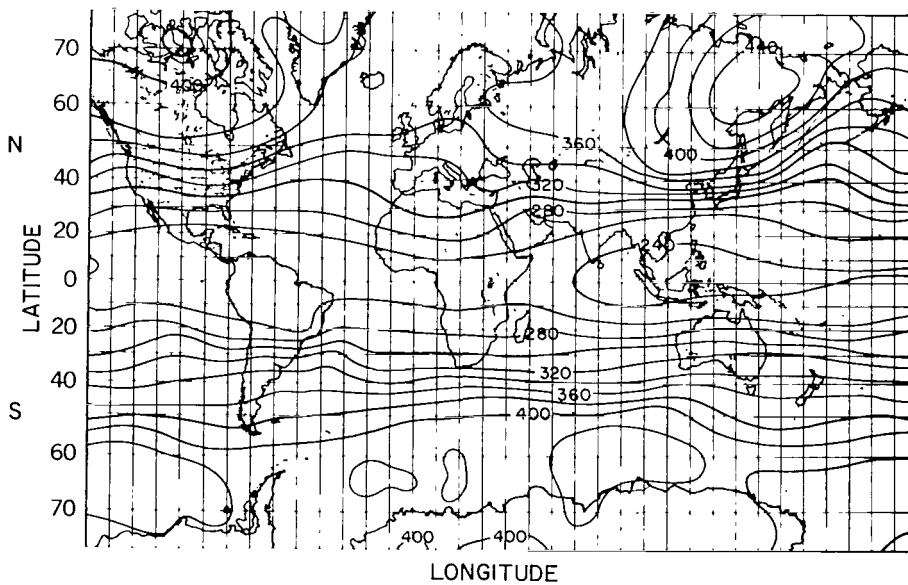

Figure 21. Global distribution of total ozone (Dobson units) derived from Nimbus-4 IRIS measurements for November 1970.
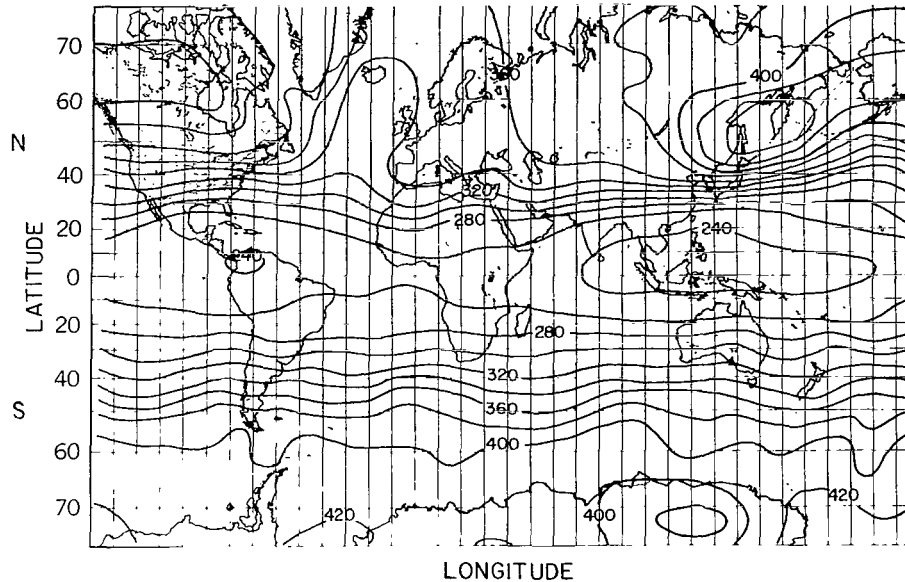
Figure 22. Global distribution of total ozone (Dobson units) derived from Nimbus-4
IRIS measurements for December 1970.

Zonal Means of Ozone

The zonal mean values of total ozone shown in figure 23 (as a function of latitude and month) reveal several subtle differences between the Northern and Southern Hemispheres. The maximum and minimum in total ozone over the middle and high latitudes of the Northern Hemisphere appear in the spring and fall months, respectively. The tropics appear to be in opposite phase. The midlatitudes of the Southern Hemisphere show a maximum in spring and minimum in fall, but the south polar region reveals quite a different seasonal change. The maximum occurs between October and November and the minimum occurs during September. This process creates the impression that the south polar region is screened from the middle latitude from June to October. An examination of the standard deviation of temperature in this hemisphere, particularly at 100 and 50 mbar, reveals a striking resemblance to the zonal mean ozone with the ozone field lagging in time by about two months.

Standard Deviation of Ozone

The standard deviation of ozone in the tropics is generally small, (about 10 D.U.) throughout the year, as shown in figure 23. This compares, in magnitude, to the annual change in total ozone. The standard deviations in the middle and high latitudes of the Northern and Southern Hemispheres are quite large, reaching a maximum of about 50 D.U. It should be noted that the occurrence of the maximum in standard deviation of ozone in the Southern Hemisphere precedes the ozone maximum, while in the Northern Hemisphere, these occur nearly simultaneously.
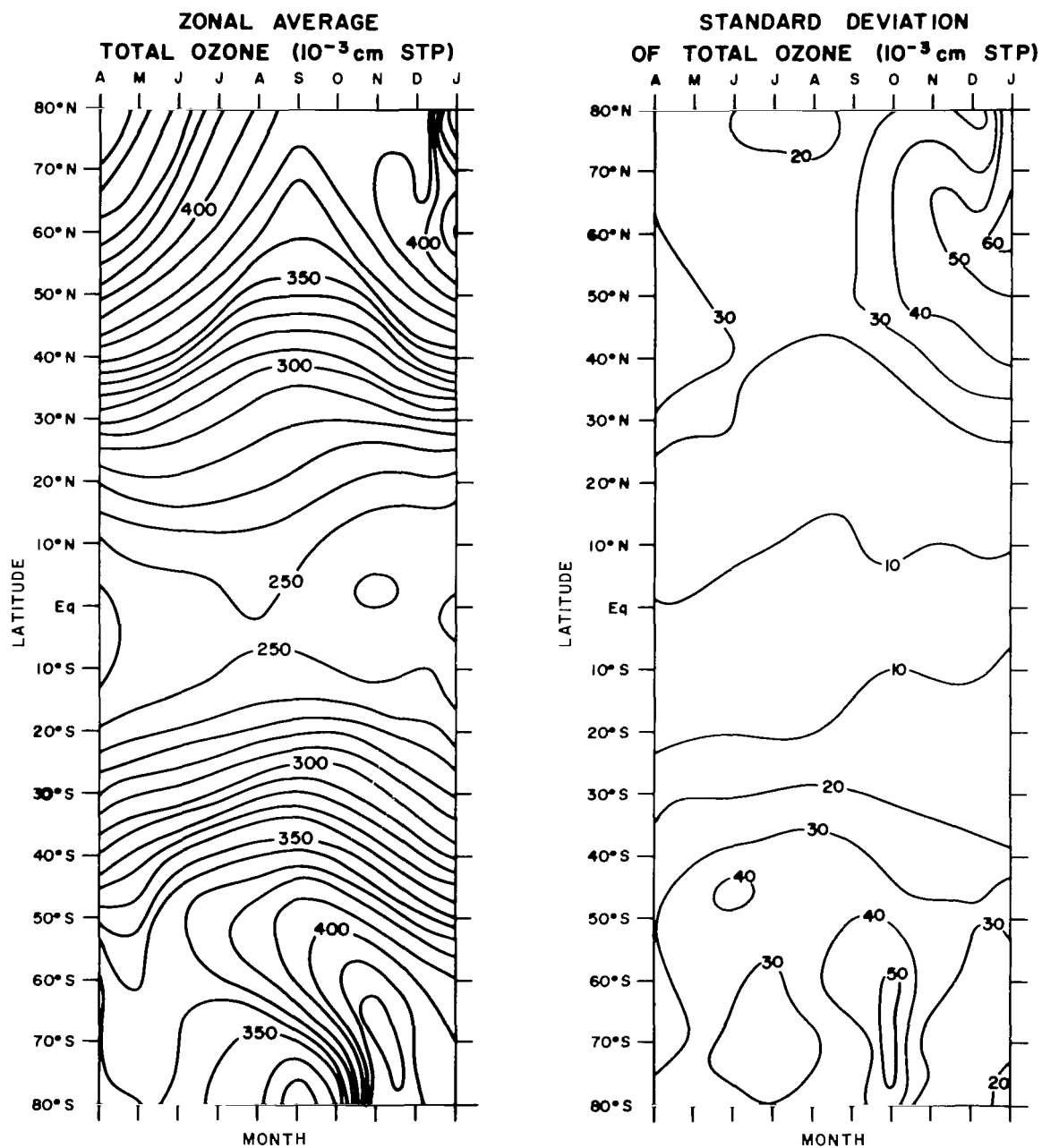
24

Figure 23. Zonal average total ozone (10^{-3}-STP) and the standard deviation of total ozone (10^{-3}-cm STP) derived from Nimbus-4 IRIS measurements for April 1970 through January 1971.

MERIDIONAL CROSS SECTIONS

The meridional cross section of the zonal mean temperature and its standard deviation are shown in figure 24 for December and January to emphasize the character of the northern polar westerly vortex before it breaks down. In the Southern Hemisphere, the vortex persists through the winter and eventually collapses during spring. The cross sections for September and October are shown in figure 25 to illustrate the behavior of the vortex in the south. The total ozone is also shown as a function of latitude at the bottom of the cross section for the standard deviation.

The polar westerly vortex in the Northern Hemisphere differs from that of the Southern Hemisphere. The standard deviation in temperature associated with the northern hemispheric vortex is observed to persist with little attenuation up to the 10-mbar level while in the south, it reaches a maximum in the lower stratosphere. The mean temperature field in the Southern Hemispheric cross sections for September and October reveal a rising motion near 30°S and a sinking motion about 60°S. This feature is not apparent in the Northern Hemisphere during December and January. The total ozone reaches a distinct maximum near 60°S, while in the north, such a feature is not conspicuous.

DISCUSSION OF THE TEMPERATURE AND OZONE OBSERVATIONS IN THE LOWER STRATOSPHERE

The solar heating, infrared radiative cooling, and transport of heat by atmospheric motions govern the thermal field in the stratosphere. Inversely, the atmospheric ozone is controlled by photochemical production and destruction, and by transport processes. Thus, a combination of the temperature and total ozone data obtained by Nimbus-4 IRIS provides a comprehensive picture of the stratospheric circulation.

A descriptive account of the temperature and ozone data is given in the earlier sections. From that description, it may be inferred that the lower stratospheric temperature field is strongly influenced by the tropospheric motions. The long planetary and standing waves generated by land-ocean configuration and orography persist up to about 30 mbar. Solar control of the thermal field begins to dominate above that level. Total ozone acts as a good tracer of the lower stratospheric motions, because it is abundant and a fairly conservative constituent at this level. Indeed, this is well borne out by the ozone maps shown earlier which resemble the temperature maps at 50 and 100 mbar.

In the tropics, the total ozone data indicate a systematic seasonal change with a maximum in July and August and also a stationary wave pattern persisting throughout the year with a maximum over the Atlantic region and a minimum over Southeast Asia. This information is not readily revealed by the temperature maps. Thus, it appears that the total ozone measurements over the tropics can be useful in climatological forecasts of the large-scale circulation in the tropics.

Figure 24. Meridional upper tropospheric and lower stratospheric cross section of zonally averaged temperature (K) and the standard deviation of temperature (K) between 80°N and 80°S latitude, derived from Nimbus-4 IRIS measurements for December 1970 and January 1971. Below the standard-deviation meridional cross section is the zonally averaged total ozone (10^{-3}-cm STP) between 80°N and 80°S latitude for the given month.
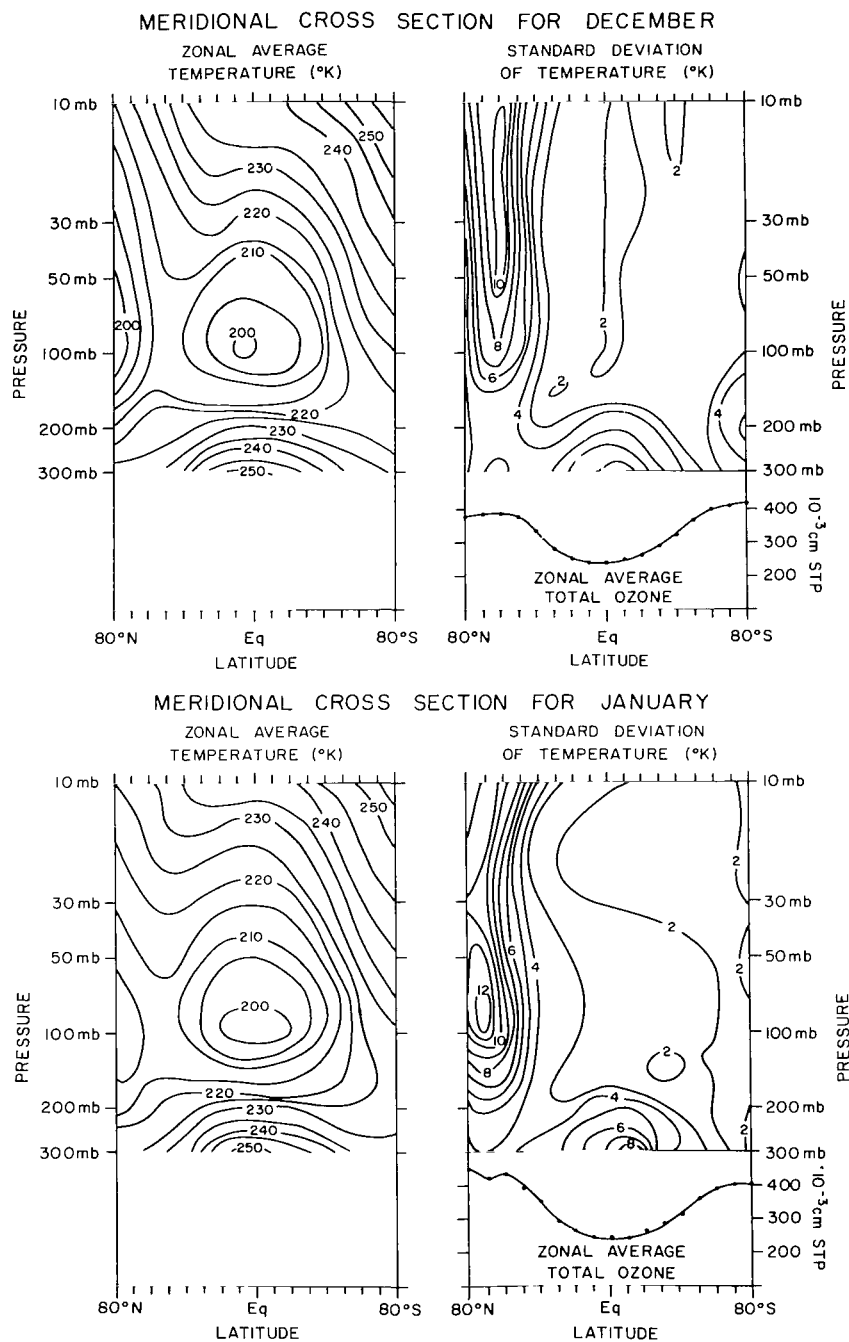
27

Figure 25. Meridional upper tropospheric and lower stratospheric cross section of zonally averaged temperature (K) and the standard deviation of temperature (K) between 80°N and 80°S latitude, derived from Nimbus-4 IRIS measurements for September and October 1970. Below the standard-deviation meridional cross section is the zonally averaged total ozone (10^{-3}-cm STP) between 80°N and 80°S latitude for the given month.
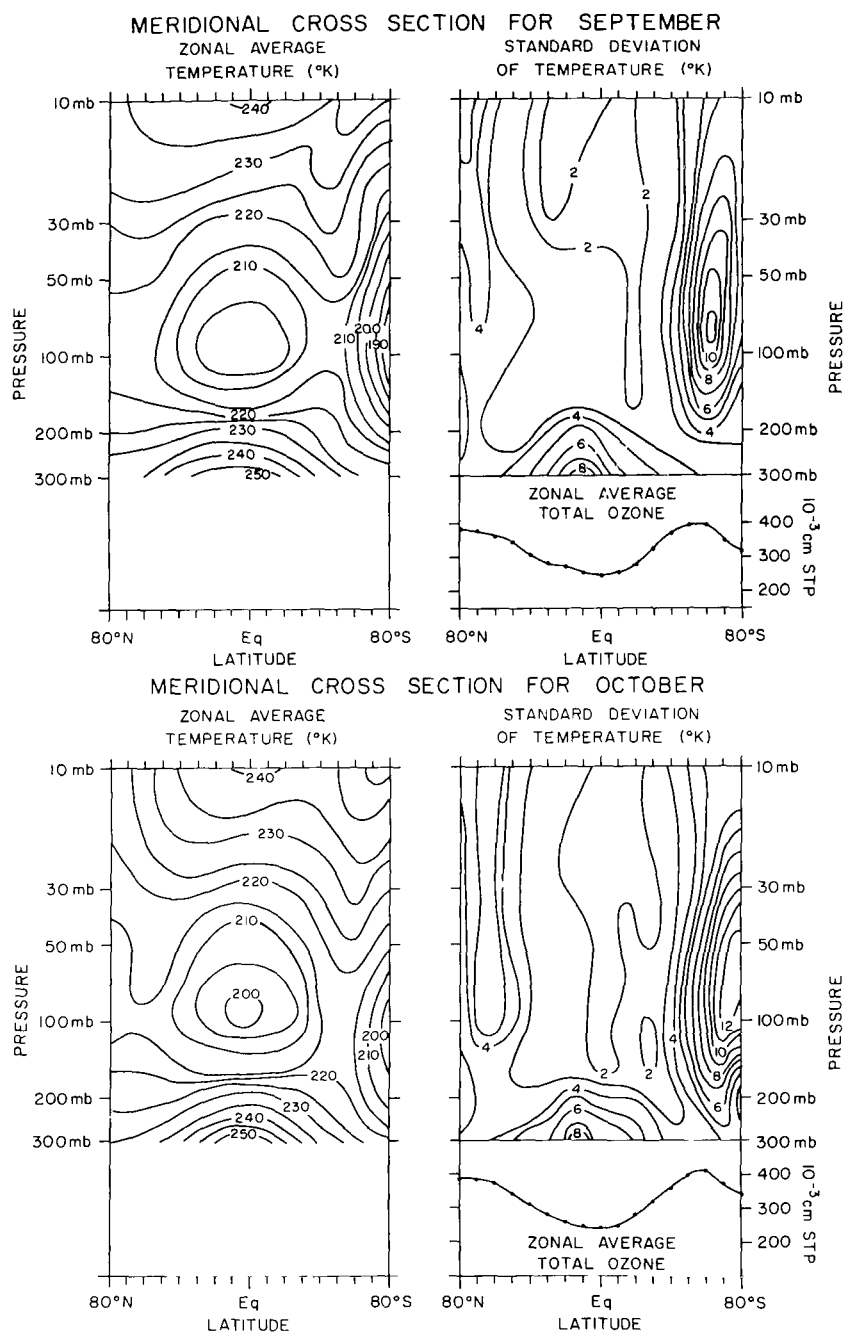
28

The stratospheric warmings that are produced in the winter season over the Northern Hemisphere at high latitudes are believed to be induced by strong forcing from the troposphere (see, for example, Matsuno, 1970, and Simmons, 1974). Despite the fact that middle winter warmings are absent in the Southern Hemisphere lower stratosphere, the Southern Hemispheric winter polar westerly vortex is considerably stronger than that of the Northern Hemisphere. This can be inferred from the IRIS temperature data. However, final warming of the Southern Hemisphere does take place in spring analogous to the spring in the Northern Hemisphere. This peculiar behavior of the Southern Hemisphere polar winter vortex is not fully explained. Labitske and Van Loon (1972) suggest that the tropospheric forcing, as revealed by the 500-mbar height field, is at a maximum in September and not in the winter months of the Southern Hemisphere. The oceans, with their larger heat reservoirs, control the Southern Hemispheric circulation systems, and hence, may be responsible for this delay. The IRIS temperature data lend support to this idea. In addition, the IRIS total ozone and standard deviation of temperature data (see figures 13 and 23) strongly suggest that the horizontal eddy transport from middle latitudes is inhibited toward the South Pole throughout the winter season. The cold Antarctic plateau, with its strong vertical stability, inhibits the eddy transfer by waves. Apparently, the eddy transfer in the south polar region resumes in spring, leading to the ozone maximum in November. In conclusion, the IRIS temperature and ozone data implicitly reveal the influences of the oceanic regime and the Antarctic plateau.

The total ozone data deduced from IRIS compare very favorably with those of the backscatter ultraviolet (BUV) spectrometer (D. Heath, GSFC, private communication, 1975). These IRIS ozone measurements, although derived with the help of temperature data, provide some information that is not contained in the thermal field. This is obvious from the IRIS-observed seasonal change in the ozone. On a short time scale, the temperatures in the lower stratosphere correlate well with the total ozone. It has also been shown by Prabhakara et al. (1973) that the total ozone data are highly correlated with the 200-mbar heights. As the ozone and temperature fields display independent behavior on a seasonal basis, it appears that, in principle, significant improvement in determining the pressure height field can be made by using the radiance data in both the 15- and 9.6-μm bands.

Goddard Space Flight Center
National Aeronautics and Space Administration
Greenbelt, Maryland   September 29, 1975

REFERENCES

Adler, R. F., "A Comparison of the General Circulation of the Northern and Southern Hemispheres Based on Satellite, Multi-channel Radiance Data," *MWR*, 103, 1975, pp. 52-60.

Barnett, J. J., "The Mean Meridional Temperature Behavior of the Stratosphere from November 1970 to November 1971 Derived from Measurements by the Selective Chopper Radiometer on Nimbus IV," *Q. J. Roy. Met. Soc.*, 100, 1974, pp. 505-530.

Bojkov, R. D., "Planetary Features of the Total Ozone and Vertical Distribution During IQSY, Part 1," *Idojaras* (Budapest), 1968, pp. 140-152.

Conrath, B. J., "Vertical Resolution of Temperature Profiles Obtained from Remote Radiation Measurements," *J. Atmo. Sci.*, 29, 1972, pp. 1262-1271.

Crutcher, H. L., "Selected-level Heights, Temperatures, and Dew Point Temperatures for the Northern Hemisphere," NAVAIR 50-1C-52 rev., Chief, Naval Operations, Washington, D. C., 1970.

Dutsch, H. V., "Atmospheric Ozone and Ultraviolet Radiation," *World Survey of Climatology*, 4, *Climate of the Free Atmosphere* (Elsevier, New York), 392 pp., 1969.

Hanel, R. A., B. J. Conrath, V. G. Kunde, C. Prabhakara, I. Revah, V. V. Salomonson, and G. Wolford, "The Nimbus 4 Infrared Spectroscopy Experiment 1. Calibrated Thermal Emission Spectra," *J. Geophys. Res.*, 77, 1972, pp. 2629-2641.

Labitske, K. and H. Van Loon, "The Stratosphere in the Southern Hemisphere. Meteor. of the Southern Hemisphere," *Meteor. Monographs*, 13 (35), 1972, pp. 113-138.

London, J., "The Distribution of Total Ozone in the Northern Hemisphere," *Beitr-Physik Atmosphare*, 36, 1963, pp. 254-263.

Matsuno, T., "Vertical Propagation of Stationary Planetary Waves in the Winter Northern Hemisphere," *J. Atmo. Sci.*, 27, 1970, pp. 871-883.

Prabhakara, C., B. J. Conrath, R. A. Hanel, and E. J. Williamson, "Remote Sensing of Atmospheric Ozone Using the 9.6 μm Band," *J. Atmo. Sci.*, 27, 1970, pp. 689-697.

Prabhakara, C., B. J. Conrath, R. A. Hanel, and V. G. Kunde. "Elimination of Cloud Effects in Sensing Ozone from 9.6 μm Band," *Proceedings of the Conference on Atmospheric Radiation*, August 1972, Fort Collins, Colo., Amer. Meteor. Soc., 1972, pp. 169-172.

Prabhakara, C., E. B. Rodgers, and V. V. Salomonson, "Remote Sensing of the Global Distribution of Total Ozone and the Inferred Upper-tropospheric Circulations from Nimbus IRIS Experiments 1," *Pure and Applied Geophysics,* **106-108**, 1973, pp. 1226-1237.

Quiroz, R. S., "The Stratospheric Evolution of Sudden Warmings in 1969-74 Determined from Measured Infrared Radiation Fields," *JAS,* **32**, 1975, pp. 211-224.

Simmons, A. J., "Planetary-scale Disturbances in the Polar Winter Stratosphere," *Quart. J. R. Met. Soc.,* **100**, 1974, pp. 76-108.

APPENDIX

The bulk of the atmospheric ozone is primarily present in the lower stratosphere at low pressures. Further, it is generally observed that increases in total ozone occur mainly due to enrichment of the ozone content in the layers immediately below the ozone maximum (Craig, 1950). This leads to an approximate relationship between the total ozone and the weighted mean pressure, $\bar{P}$, of the ozone layer as defined below:

$$\bar{P} = \frac{\int P(z) \, O_3(z) \, dz}{\int O_3(z) \, dz} \qquad (1)$$

where $O_3(z)$ is the ozone concentration and $P(z)$ is the atmospheric pressure at any height z. In the present study, it is assumed that the total ozone increases linearly as the weighted mean pressure, $\bar{P}$, increases, that is

$$O_3^T(\bar{P}) = O_3^T(P_m) + C(\bar{P} - P_m) \qquad (2)$$

where

O_3^T = total ozone,

P_m = the known mean pressure of the ozone layer (P_m = 40 mbar), and

C = a constant (equal to 0.0058 cm of ozone per mbar of pressure) chosen from climatological data of ozone profiles reported by Hering and Borden (1967).

The idea expressed in equation 2 stems from a study reported by Miller (1960). This total ozone model effectively allows the representation of the vertical ozone profile by one parameter; namely, its weighted mean pressure, $\bar{P}$.

Infrared absorption by atmospheric ozone in the 9.6-μm band depends linearly on the total amount of ozone and also on the weighted mean pressure. The $\bar{P}$ of the ozone model described above can then be related to the infrared absorption properties of the ozone layer in a simple fashion.

The method of estimating total ozone amounts to determining the weighted mean pressure $\bar{P}$ from the strength of the 9.6-μm ozone band, as follows: From the radiative transfer equation relating to the up-welling intensity I at a given wave number

$$I = B_0 \tau_0 + \int_{\tau_0}^{1} B \, d\tau \qquad (3)$$

33

where

B_o = the Planck intensity emitted by the bottom surface,

τ_o = the transmission of the atmosphere from the top to the surface, and

τ = the transmission from the top to any other level in the atmosphere.

Equation 3 can be simplified as

$$I = B_o \tau_o + \bar{B} (1 - \tau_o)$$

that is

$$(B_o - I) = (B_o - \bar{B})(1 - \tau_o) \tag{4}$$

where

$$\bar{B} = \frac{\int B(z)\, O_3(z)\, dz}{\int O_3(z)\, dz}$$

is weighted mean emission of the ozone layer.

The definition of $\bar{P}$ and $\bar{B}$ is such that they would both correspond closely to the same height in the atmosphere.

From the model of the ozone profile and from the nature of the absorption in the 9.6-μm region, we can relate the absorption A of the ozone layer linearly to the total amount of ozone as

$$A \left[(O_3^T (\bar{P}))\right] = (1 - \tau_o) = k\, O_3^T (\bar{P}) \tag{5}$$

where k is some effective absorption coefficient. It has been found that the value of k applicable to the total band is 0.425.

Substituting equations 2 and 5 into equation 4, we get

$$(B_o - I) = (B_o - \bar{B})\, k\, O_3^T (\bar{P})$$

$$= (B_o - \bar{B})\, k\, \left[O_3^T (Pm) + C (\bar{P} - Pm)\right] \tag{6}$$

The left-hand side of this equation is known from the 11-μm and 9.6-μm IRIS measurements. On the right-hand side, B is known as a function of pressure in the atmosphere from the retrieved temperature profile. Thus, we can solve for $\bar{P}$ iteratively from equation 6 by assuming B at that level is equal to $\bar{B}$. From $\bar{P}$, the total ozone is estimated with equation 2.

This simple method is tested against the more detailed total ozone sensing technique reported in Prabhakara et al. (1970) and is found to be consistent to within a few Dobson units.

REFERENCES

Craig, R. A., "The Observations and Photo-chemistry of Atmospheric Ozone and Their Meteorological Significance," *Meteor. Monographs,* 1 (2), Amer. Meteor. Soc.., Boston, Mass., 1950.

Hering, W. S. and T. R. Borden, *Ozone Sonde Observations over North America,* AFCRL-46-30(IV), Air Force Cambridge Research Laboratories, Bedford, Mass., 1967.

Miller, L. E., "Atmospheric Gases," *Handbook of Geophysics,* The Macmillan Co., New York, 1960.

Prabhakara, C., B. J. Conrath, R. A. Hanel, and E. J. Williamson, "Remote Sensing of Atmospheric Ozone Using the 9.6 μm Band," *J. Atmo. Sci.,* 27, 1970, pp. 689-697.

"The aeronautical and space activities of the United States shall be conducted so as to contribute . . . to the expansion of human knowledge of phenomena in the atmosphere and space. The Administration shall provide for the widest practicable and appropriate dissemination of information concerning its activities and the results thereof."

—NATIONAL AERONAUTICS AND SPACE ACT OF 1958

NASA SCIENTIFIC AND TECHNICAL PUBLICATIONS

TECHNICAL REPORTS: Scientific and technical information considered important, complete, and a lasting contribution to existing knowledge.

TECHNICAL NOTES: Information less broad in scope but nevertheless of importance as a contribution to existing knowledge.

TECHNICAL MEMORANDUMS: Information receiving limited distribution because of preliminary data, security classification, or other reasons. Also includes conference proceedings with either limited or unlimited distribution.

CONTRACTOR REPORTS: Scientific and technical information generated under a NASA contract or grant and considered an important contribution to existing knowledge.

TECHNICAL TRANSLATIONS: Information published in a foreign language considered to merit NASA distribution in English.

SPECIAL PUBLICATIONS: Information derived from or of value to NASA activities. Publications include final reports of major projects, monographs, data compilations, handbooks, sourcebooks, and special bibliographies.

TECHNOLOGY UTILIZATION PUBLICATIONS: Information on technology used by NASA that may be of particular interest in commercial and other non-aerospace applications. Publications include Tech Briefs, Technology Utilization Reports and Technology Surveys.

Details on the availability of these publications may be obtained from:

SCIENTIFIC AND TECHNICAL INFORMATION OFFICE

NATIONAL AERONAUTICS AND SPACE ADMINISTRATION

Washington, D.C. 20546